

# The WARPS Survey: VI. Galaxy Cluster and Source Identifications from Phase I

Eric S. Perlman<sup>1,7,9,11,12,13,14,15</sup>, Donald J. Horner<sup>2,8,11,12</sup>, Laurence R. Jones<sup>3,11,13,14,15</sup>, Caleb A. Scharf<sup>1,10,12</sup>, Harald Ebeling<sup>4,13,14,16</sup>, Gary Wegner<sup>5,17</sup>, and Matthew Malkan<sup>6,15</sup>

## ABSTRACT

---

<sup>1</sup>Space Telescope Science Institute, 3700 San Martin Drive, Baltimore, MD 21218, USA

<sup>2</sup>Laboratory for High Energy Astrophysics, Code 662, Goddard Space Flight Center, Greenbelt, MD 20771, USA

<sup>3</sup>School of Physics & Astronomy, University of Birmingham, Birmingham B15 2TT, UK

<sup>4</sup>Institute for Astronomy, 2680 Woodlawn Drive, Honolulu, HI 96822, USA

<sup>5</sup>Department of Physics and Astronomy, Dartmouth College, 6127 Wilder Laboratory, Hanover, NH 03755, USA

<sup>6</sup>Department of Physics and Astronomy, University of California, Los Angeles, CA 90024, USA

<sup>7</sup>Department of Physics and Astronomy, Johns Hopkins University, 3400 North Charles Street, Baltimore, MD 21218, USA

<sup>8</sup>Department of Astronomy, University of Maryland, College Park, MD 20742, USA

<sup>9</sup>Department of Physics, University of Maryland - Baltimore County, 1000 Hilltop Circle, Baltimore, MD 21250, USA

<sup>10</sup>Columbia Astrophysics Laboratory, Columbia University, Mail Code 5247, 550 West 120th Street, New York, NY 10027, USA

<sup>11</sup>Guest Observer at Kitt Peak National Observatory. KPNO/NOAO is operated by the Association of Universities for Research in Astronomy (AURA), Inc. under cooperative agreement with the National Science Foundation

<sup>12</sup>Guest Observer at Cerro Tololo Inter-American Observatory. CTIO is operated by the Association of University for Research in Astronomy (AURA), Inc. under cooperative agreement with the National Science Foundation

<sup>13</sup>Guest Observer at the Canada-France-Hawaii Telescope. CFHT is operated by the National Research Council of Canada, the Centre National de la Recherche Scientifique de France, and the University of Hawaii

<sup>14</sup>Guest Observer at the W. M. Keck Observatory. The W.M. Keck Observatory is operated as a scientific partnership among the California Institute of Technology, the University of California and the National Aeronautics and Space Administration.

<sup>15</sup>Guest Observer at Lick Observatories. Lick Observatory is operated by the University of California.

<sup>16</sup>Observer at the University of Hawaii 2.2m telescope on Mauna Kea.

<sup>17</sup>Observer at the Michigan-Dartmouth-MIT Observatory.

We present in catalog form the optical identifications for objects from the first phase of the Wide Angle ROSAT Pointed Survey (WARPS). WARPS is a serendipitous survey of relatively deep, pointed ROSAT observations for clusters of galaxies. The X-ray source detection algorithm used by WARPS is Voronoi Tessellation and Percolation (VTP), a technique which is equally sensitive to point sources and extended sources of low surface brightness. WARPS-I is based on the central regions of 86 ROSAT PSPC fields, covering an area of 16.2 square degrees. We describe here the X-ray source screening and optical identification process for WARPS-I, which yielded 34 clusters at  $0.06 < z < 0.75$ . Twenty-two of these clusters form a complete, statistically well defined sample drawn from 75 of these 86 fields, covering an area of 14.1 square degrees, with a flux limit of  $F(0.5 - 2.0 \text{ keV}) = 6.5 \times 10^{-14} \text{ erg cm}^{-2} \text{ s}^{-1}$ . This sample can be used to study the properties and evolution of the gas, galaxy and dark matter content of clusters, and to constrain cosmological parameters. We compare in detail the identification process and findings of WARPS to those from other recently published X-ray surveys for clusters, including RDCS, SHARC-Bright, SHARC-south and the CfA 160 deg<sup>2</sup> survey.

## 1. Introduction

Clusters of galaxies represent the largest gravitationally bound structures in the universe. Their space density and evolution strongly constrain hierarchical structure formation models, which postulate that the most massive clusters form via mergers of less massive clusters. The measurement of the X-ray temperature and luminosity functions (XTF and XLF) of clusters of galaxies are powerful discriminants between hierarchical models of structure formation (e.g., Kaiser 1991), which can provide strong constraints on cosmological models (e.g., Bahcall & Cen 1992; Viana & Liddle 1996; Carlberg et al. 1997). In order to study the distribution of massive clusters in the universe, as well as their characteristics, it is crucial to compile large, relatively unbiased samples of clusters.

One of the least biased ways to select a sample of clusters with properties directly translatable to the size of the mass aggregation, is via X-ray surveys. The X-ray emission in clusters originates in primordial gas and material stripped from the galaxies in the clusters, and scales directly with the density and temperature of the emitting gas (Jones & Forman 1984), which in turn are strongly correlated with the gravitating mass (Horner et al. 1999). Optical surveys, by comparison, are strongly affected by projection effects (Lucey 1983; Struble & Rood 1991; Sutherland 1988; Frenk et al. 1990; van Haarlem et al. 1997). Moreover,

a number of studies have found that the optical properties of clusters (e.g., richness) are not very good indicators of cluster mass (Frenk et al. 1990).

The Wide-Angle ROSAT Pointed Survey (WARPS; Scharf et al. 1997, hereafter Paper I; Jones et al. 1998, hereafter Paper II; Ebeling et al. 2001b, hereafter Paper III; Fairley et al. 2000, hereafter Paper IV, Ebeling et al. 2001a, hereafter Paper V) was designed to compile a representative, X-ray selected sample of clusters of galaxies. Groups of galaxies and individual galaxies are also detectable in WARPS, to somewhat lower redshifts than clusters (out to  $z \sim 0.2 - 0.3$  and  $z \sim 0.05$ , respectively, compared to  $z > 1$  for clusters). WARPS uses the Voronoi Tessellation and Percolation (VTP, Ebeling 1993; Ebeling & Wiedenmann 1993) algorithm to detect both extended and point-like X-ray sources. Our application of VTP to detect X-ray sources has been described in Paper I, as has the survey calibration. An extensive optical follow-up program (described in detail in Paper II) imaged not only extended X-ray sources (which are the most promising cluster candidates) but also all blank field point X-ray sources, and then took spectra of galaxies in the fields of cluster candidates. We assume that groups and clusters of galaxies form a continuous population, referred to simply as “clusters,” and do not further distinguish between groups and clusters of galaxies.

Early measurements of the cluster XLF, based on EXOSAT data (Edge et al. 1990) and the *Einstein* Extended Medium Sensitivity Survey (EMSS, Henry et al. 1992), indicated strong negative evolution at  $L(0.3 - 3.5 \text{ keV}) > 10^{44} \text{ erg s}^{-1}$ , perhaps even at relatively low redshifts. This was seen as support for critical density, cold dark matter cosmologies (e.g., Viana & Liddle 1996). However, a large number of recent results have changed the picture substantially. At low redshift ( $z < 0.3$ ), the results of the ROSAT Brightest Cluster Sample (BCS, Ebeling et al. 1997) show little if any evolution of the cluster XLF. At higher redshift, both new ROSAT surveys (RDCS, Rosati et al. 1998; WARPS, Papers II, III; SHARC-south Burke et al. 1997; SHARC-Bright Romer et al. 2000; CfA 160  $\text{deg}^2$  [also known as VMF], Vikhlinin et al. 1998b; NEP, Mullis 2000) and re-analyses of EMSS data (Nichol et al. 1997, Stocke et al., in preparation) are again consistent with no evolution at  $z < 1$  (except perhaps at the highest luminosities; see in particular Rosati et al. 1998; Vikhlinin et al. 1998a). The reason for this discrepancy is a subject of active debate, but contributing factors may include underestimation of X-ray flux by the EMSS (Papers II, III), and misidentification of some EMSS X-ray sources as clusters (Nichol et al. 1997; Rector et al. 1999). Indeed, the most current analysis of the highest-redshift part of the EMSS sample (Luppino & Gioia 1995) is also consistent with no significant evolution between  $z \sim 0.33$  and  $z \sim 0.75$  (see also Paper III; although for a somewhat different view of the same literature see Gioia et al. 2001).

Here we describe the identification process and present in catalog form optical identifications for objects from the first phase of the WARPS project (WARPS-I), which

included data from 86 ROSAT Position Sensitive Proportional Counter (PSPC) fields. This sample formed the basis of Papers I and II. The optical identifications for galaxy clusters from WARPS-I are essentially complete. Papers III, IV, and V also include data from the second phase of the WARPS project (WARPS-II), which includes nearly 4 times as many PSPC fields and concentrates on the most distant clusters. Those identifications are almost complete and will be presented elsewhere (Horner et al. in preparation).

In § 2 we describe briefly the survey methods and source identification process, as well as cross-correlations with various astronomical databases. In § 3 we comment explicitly on the efficacy of VTP as a method for detecting clusters of galaxies, and compare it with other X-ray source detection methods currently in use. In § 4 we describe the statistically complete, flux limited WARPS-I sample of clusters of galaxies, and also comment on individual clusters and interesting sources which fall below the flux limit. We conclude in § 5 by outlining future directions for research with this and other cluster samples.

Unless otherwise stated, we use  $q_0 = 0.5$  and  $H_0 = 50 \text{ km s}^{-1} \text{ Mpc}^{-1}$  when calculating distance dependent quantities. Similarly, we use the 0.5–2.0 keV ROSAT PSPC band when quoting count rates, fluxes, and luminosities unless otherwise noted. The catalogs, finder charts, and other information can be found on our WARPS WWW page at <http://lhea-www.gsfc.nasa.gov/~horner/warpsI/warpsI.html>.

## 2. Survey Methods

The WARPS-I sample was drawn from 86 ROSAT PSPC pointings, covering a total area of  $16.2 \text{ deg}^2$ . These fields were selected at random from ROSAT observations with exposure times greater than 8 ks and Galactic latitude  $|b| > 20^\circ$ . Fields centered on bright star clusters or nearby bright galaxies such as M31 were excluded. This sample was used in Paper II. However, a more restrictive field selection has subsequently been applied to make WARPS-I consistent with WARPS-II. This selection process excluded 11 fields, so that the statistically complete sample is now drawn from 75 ROSAT fields ( $14.1 \text{ deg}^2$ ). Four fields (rp200510, rp400117, rp700257, and rp700302) were dropped due to their high background level. One field (rp600097) was discarded due to the presence of the large optical target, NGC 600. Five other fields (rp8000003, rp800150a01, rp800401a01, rp800471n00, and rp800483n00) were dropped since the pointing targets are galaxy clusters. One ROSAT field originally included in the sample, rp700305, was subsequently split in the archive into two separate fields, rp700305a00 and rp700305a01, each with exposure time less than 8ks. Since it is our policy not to combine fields, we have dropped this field from consideration. Any clusters found in the dropped fields as part of the optical follow-up are reported here, but

they are not considered part of the statistically complete sample. In Table 1, we list all fields included in WARPS-I.

## 2.1. X-ray Source Detection

In each PSPC field we utilized the annulus between  $3'$  and  $15'$  radius. At the outer limit this ensures that the point-spread function (PSF), the size of which increases with radius, has a FWHM of  $< 45''$ , and also avoids areas strongly shaded by the PSPC window support structure. At the inner limit, this avoids the target of each pointing. We used only photons in the 0.5–2.0 keV band for source detection and measurement of fluxes. This minimizes both the size of the PSF and background relative to typical cluster spectra.

The VTP algorithm (Ebeling 1993; Ebeling & Wiedenmann 1993) was used for X-ray source detection. VTP is a general method for detecting non-Poissonian structure in a two-dimensional event distribution. In the case of detected photons, VTP will detect all regions of enhanced surface brightness. The implementation of VTP has previously been described in Papers I and II; here we discuss only the most important points.

The Voronoi tessellation is composed by defining each photon as the center of a cell polygon whose sides form the perpendicular bisectors of the non-crossing vectors joining the nearest neighbor photons. The surface brightness associated with this cell equals the number of photons in the cell (one, unless several photons were registered in the same PSPC resolution element) times the inverse of the product of cell area and local exposure time. To account for the non-uniform exposure of each PSPC field, we constructed exposure maps in two energy bands (0.5–0.9 and 0.9–2.0 keV), using an algorithm based on the work of Snowden et al. (1992). This resulted in an improvement of up to 10-15% in the computation of source fluxes. VTP then searches for brightness enhancements by comparing the cumulative surface brightness distribution with the expectation from a Poisson distribution, and finds a global threshold for the surface brightness distribution in a given field at which the observed distribution becomes inconsistent with random noise. In the percolation step of the VTP analysis, the algorithm groups into sources all adjacent cells whose surface brightness exceeds the threshold value. Sources consisting of very few photons consistent with random fluctuations are discarded; for the remainder VTP computes source properties, such as source position, count rate, and signal-to-noise ratio.

In using VTP, we set a lower limit in count rate of  $3 \times 10^{-3}$  ct/s for inclusion in the preliminary sample, corresponding to a flux of approximately  $3.5 \times 10^{-14}$  ergs cm $^{-2}$  s $^{-1}$  in the 0.5–2.0 keV band. However, our final limit in *total flux* (*i.e.*, corrected for the component

below our detection threshold) is  $6.5 \times 10^{-14}$  ergs cm $^{-2}$  s $^{-1}$  in the 0.5–2.0 keV band. This flux limit is slightly higher than that chosen in Paper II ( $6.0 \times 10^{-14}$  ergs cm $^{-2}$  s $^{-1}$ ) to be sure of completeness; it was chosen as a result of the simulations described in Paper I, which tested both the threshold at which we could reliably label a source as extended as well as the typical sizes of the flux corrections we applied for extended sources.

VTP was run five times on each field using different surface brightness thresholds in order to distinguish real single sources from those composed of blends of several sources (point-like or extended). This also reduces uncertainties in the count rate of sources close to, and occasionally blended with, positive background fluctuations. We then selected the optimal surface brightness threshold for each field by visually inspecting the VTP source photon distribution for each of the five thresholds. This procedure not only allowed us to separate sources blended together at low percolation thresholds, but also permitted us to identify and merge complex extended sources split into several fainter sources at high percolation thresholds (cf. §3).

The list of deblended sources and respective VTP parameters were then passed to an algorithm that estimates their true total flux. To do this, one must make assumptions about source morphology. We chose to assume that sources are either intrinsically point-like or follow a King profile with  $\beta = 2/3$ ; normalization and core radius are free parameters determined from the VTP source parameters. For each source, we then computed two flux estimates,  $S_{\text{King}}$  and  $S_{\text{point}}$ , under the above assumptions. We classify an object as extended if its extent parameter  $f_{\text{ext}}$ , defined as the ratio  $S_{\text{King}}/S_{\text{point}}$ , lies above 1.2, and “marginally extended” if  $1.1 < f_{\text{ext}} < 1.2$ .

In Table 2, we list all sources found by VTP with fluxes  $F_x \geq 6.5 \times 10^{-14}$  ergs cm $^{-2}$  s $^{-1}$ . Table 3 lists sources at lower fluxes and in fields that did not qualify for the complete sample. Optical images and spectra were not obtained for every X-ray source, as described in §2.2, so for the non-cluster candidates (*e.g.*, AGN, § 2.4) our identification process cannot be regarded as complete. Only 40% of all sources were identified either from the literature or through follow-up observations. The columns in Tables 2 and 3 are as follows:

1. The assigned source name.
2. The ROSAT pointing containing the source.
3. The right ascension (hours, minutes, seconds) in J2000 coordinates (typical error is 15”).
4. The declination (degrees, minutes, seconds) in J2000 coordinates (typical error is 15”).

5. The raw VTP count rate in units of  $10^{-3}$  counts per second.
6. The corrected (i.e., total) VTP count rate in units of  $10^{-3}$  counts per second.
7. The Galactic hydrogen column density ( $N_H$ ) in units of  $10^{20}$   $\text{cm}^{-2}$  from Dickey & Lockman (1990).
8. The unabsorbed X-ray flux in units of  $10^{-13}$   $\text{ergs cm}^{-2} \text{ s}^{-1}$  in the 0.5–2.0 keV band. For clusters of galaxies, the flux was calculated using the same iterative method used by Ebeling et al. (1998). We assume a Raymond-Smith spectrum with a redshift appropriate for each cluster and metal abundance of 0.3 solar. The temperature of the model was derived iteratively by constraining the cluster to obey the observed  $L - T$  relation (White, Jones & Forman 1997). Fluxes were obtained for AGN and unidentified sources assuming a power law spectrum with  $F_\nu \propto \nu^{-1}$ . The flux for sources identified as stars was calculated assuming a Raymond-Smith model with a temperature of  $2 \times 10^6$  K and no correction for Galactic hydrogen column density.
9. The extent parameter as discussed above.
10. The imaging status of the source. The letter indicates the band of the optical image(s) obtained.
11. The status of the spectroscopic follow-up. A 'Y' indicates that spectra were taken for this source.
12. The identification of the source (e.g., cluster, AGN, star). Identifications in lower case were identified based on the literature (primarily using NED and SIMBAD) while upper case IDs are based on WARPS optical follow-up observations. Sources listed as blends are briefly discussed in the notes column.
13. The redshift of the source, if known, or spectral type for stars.
14. Alternate names and other notes. Sources listed as SHARC appear in the SHARC Bright Survey catalog (Romer et al. 2000). Sources listed as VMF correspond to sources in the CfA 160  $\text{deg}^2$  survey of Vikhlinin et al. (1998b). Sources listed as RIXOS correspond to sources in the RIXOS survey catalog (Mason et al. 2000). NVSS (Condon et al. 1998) and FIRST (e.g., White et al. 1997) radio sources are also indicated.

In Figure 2, we show overlays of the observed X-ray emission on digitized plates from the POSS-I, UKST, or POSS-II surveys for all 60 sources with  $F_x \geq 6.5 \times 10^{-14}$   $\text{ergs cm}^{-2} \text{ s}^{-1}$ , that are within the complete sample fields and were flagged by VTP as either extended or

marginally extended. We have also included at the end of the Figure, 4 additional X-ray sources which were classified as pointlike by VTP but were selected as cluster candidates based on optical imaging (§ 2.3.1). As discussed in §4, one of these four sources turned out to be a  $z = 0.722$  cluster. Finder charts for X-ray sources not identified as cluster candidates are available on our WWW page.

## 2.2. Optical/X-ray Selection of Cluster Candidates

In order to select sources for follow-up, it was necessary to define selection criteria for cluster candidates, as well as an integrated program of optical imaging and spectroscopy. This sub-section discusses the selection criteria, while the next sub-section discusses the optical follow-up program and how it was integrated with the selection criteria. In Paper II, we detailed the method by which we decided to image and take spectra of possible cluster candidates. Here we review the essential points.

### 2.2.1. Selection Criteria

The primary motivation for the selection criteria was to ensure the completeness of the sample of clusters of galaxies. In order to ensure maximal completeness, we followed up our deblending with a visual screening of every X-ray source. This is helpful because even after deblending, an X-ray source can have a large  $f_{ext}$  either by virtue of being truly extended or because it is a blend of two or more unresolved sources too close to be resolved by the ROSAT PSPC. It is also helpful because a finite probability exists for a truly extended source to masquerade as a point source in the VTP list, if for example it is either very core dominated (*e.g.*, an extreme cooling flow) or at very high redshifts. Finally, as noted above, sources of low surface brightness can be split up by deblending into multiple sources. Each of these effects is applicable not only to VTP but indeed to any algorithm of X-ray source detection, or any algorithm which determines source extent, as discussed in Paper II.

This procedure allowed us to sort the X-ray sources into four categories - (1) those flagged by VTP as extended which were very likely physically extended; (2) those flagged by VTP as extended which were very likely blends; (3) those flagged by VTP as point-like which were possibly extended; and (4) those flagged by VTP as point-like which were likely point-like. We then decided to accept for our first cut list of cluster candidates *every* source which might possibly be a cluster. This included not only all sources flagged by our source detection procedure as extended or marginally extended (*i.e.*, categories 1 and 2 above), but



also a significant number of sources flagged as point-like (category 3 above).

Once a candidate source list was selected, we then designed an optical follow-up program which placed particular emphasis on both completeness and reliability. Included in this list were a number of sources which eventually fell below the flux limit. The reason for this is two-fold: first of all we wanted to compile a complete cluster list, so all extended sources in phase I were followed up regardless of whether they exceeded the flux limit; and second, as our processing algorithms improved, VTP was rerun, and thus the fluxes changed slightly.

To carry out our first screening, Automatic Plate Measuring Facility (APM; see Irwin et al. 1994) measurements of Palomar  $E$  and  $O$  and UKST  $R$  and  $B_j$  plates were obtained at the positions of all X-ray sources with count rate  $> 3 \times 10^{-3}$  ct/s (0.5–2 keV) within the survey area. We also obtained the Digitized Sky Survey images of the source fields, and overlaid X-ray contours. A large fraction of the X-ray sources have obvious optical counterparts which are immediately pinpointed in this step. This also allows one to identify systematic pointing errors, which can reach  $\sim 15''$  and varies in direction from dataset to dataset (Briel & Pfeiffermann 1995). Once these overlays were made, a source was accepted as a possible cluster candidate if it met any one of three criteria:

- The X-ray source is extended or marginally extended and at least one galaxy is visible on the digitized sky survey plate, where the galaxy (ies) is not local ( $z \lesssim 0.01$ ) and of similar optical and X-ray size. In this case we not only obtained an image but immediately selected the field for spectroscopy.
- The X-ray source is extended or marginally extended and no optical counterpart is visible within one magnitude of the plate limit.
- The X-ray source is point-like but no optical counterpart is visible within one magnitude of the plate limit.

This process selected 108 sources for optical imaging. In practice some sources just below the flux limit were followed up because (a) the final fluxes depended to a small degree on the unknown source spectrum, which for clusters is based on the  $L - T$  relation and thus requires knowledge of the redshift, and (b) some source fluxes changed slightly at one point during the survey when we reran the VTP algorithm. Figure 1b shows a histogram of the extent parameters  $f_{ext}$  of the cluster candidates in the complete sample from this first screening.

### 2.2.2. *Cross-correlation with other source catalogs*

In order to identify previously known clusters, as well as AGN, Galactic stars and radio sources, we cross-correlated our source list with NED, SIMBAD and the NVSS and FIRST VLA survey lists (Condon et al. 1998, Becker et al. 1995). This produced a large number of IDs, particularly for non-cluster sources, which we list in Table 2 and 3. It also allowed us to screen out some X-ray sources we flagged as possibly extended, as more likely AGN. The cross-correlation with the NVSS revealed that 18 WARPS clusters may contain radio sources; the fluxes of these sources are listed in Table 6 (see also § 4). This is certainly not unexpected; both in the present epoch and at redshifts up to  $z = 0.8$ , approximately 30-50% of clusters contain radio galaxies, usually of the FR 1 type (Owen & Ledlow 1997; Stocke et al. 1999). In the case of optical clusters with radio sources in the field, we have checked the X-ray/optical overlays for X-ray enhancements and/or other evidence that some of the observed X-rays might be emitted by an AGN. Two such cases are noted in § 4.

We have also cross-correlated our source list with those of other ongoing ROSAT surveys, particularly those which have as their aim the discovery of clusters of galaxies (e.g., SHARC, Romer et al. 2000; CfA 160 deg<sup>2</sup>, Vikhlinin et al. 1998b). The information from these cross-correlations is given and appropriately referenced in Table 2.

## 2.3. **Optical Follow-up Program**

Once candidates for follow-up were selected according to the procedure laid out in § 2.2, we designed a program of optical imaging and spectroscopy, with a further selection step in between the imaging and spectroscopy. The goal of the optical follow-up program was to identify all clusters in the WARPS sample and determine their redshifts. The optical follow-up program used many different telescopes for imaging and spectroscopy. Our WWW page gives details of the observations for specific sources.

### 2.3.1. *Optical Imaging*

Images were obtained of cluster candidates, usually in the R band, which gives a good combination between high sensitivity, good chip cosmetics (i.e., no fringing), and sensitivity to galaxies at all but the highest redshifts where X-ray selected clusters are known (up to  $z \sim 0.9$ , where the Ca break passes out of the R band). These images were obtained at several different observatories (see the WWW page for details). Often an object was imaged more than once, either in R or I band, if the initial images revealed a still blank field, or

evidence of faint galaxies within the X-ray flux maximum region. Through this process, a total of 64 objects were found to coincide with an overdensity of galaxies and thus classified as cluster candidates.

### 2.3.2. Optical Spectroscopy

The next step in our optical follow-up was to observe spectroscopically the 64 objects identified as cluster candidates by the method described above. We also observed an additional 13 sources whose IDs are listed in Table 2. In Figure 1c, we show a histogram of the extent parameters  $f_{ext}$  of the sources selected for spectroscopy.

For each cluster candidate, we used X-ray/optical overlays to select galaxies for spectroscopy based not only upon their brightness but also their location relative to the X-ray centroid or peak(s). We attempted to associate galaxy groupings with each individual peak in the X-ray surface brightness distribution, not only to quantify the degree of possible point-source (*i.e.*, non-cluster) contamination, but also to account for superpositions of two truly extended sources. In obtaining spectra we typically used low dispersion gratings, and where possible multi-slit masks were designed in order to maximize our efficiency in identifying cluster members.

We identify an X-ray source as a cluster if (1) at least two galaxies (in the case of two or three spectra of good signal to noise) or at least three galaxies (in the case of four or more spectra) have very similar redshifts, and (2) if it can be reliably determined that the X-rays were not emitted by an AGN, star or other point source (some blends are present; see § 4.4). As a result of this program, 34 clusters were identified, 22 of which are above our flux limit of  $6.5 \times 10^{-14}$  erg cm<sup>-2</sup> s<sup>-1</sup>. In Table 4, we list information on each cluster; we will analyze the cluster population in more depth in § 4.

## 2.4. AGN in the WARPS-I sample

A significant number (22) of the objects we observed spectroscopically are AGN. These objects, along with those previously identified as AGN in other surveys (28 found via our NED and SIMBAD cross-correlations), are listed as such in Table 2. Several of these AGN are located in fields with significant galaxy overdensities, suggesting that those objects may reside in a group or cluster of galaxies. Rich environments are relatively common among AGN, particularly radio-loud AGN (e.g., Ellingson et al. 1991). A small fraction of the X-ray emission in objects of this sort might originate in a hot intracluster medium (as found for

several 3CRR quasars and radio galaxies by Hardcastle & Worrall 1999); however, we believe this fraction is too small to constitute a significant source of error in our  $\log N - \log S$  or luminosity function.

### 3. Efficacy of VTP and Comparison with Other Surveys

WARPS is one of several X-ray surveys for clusters of galaxies based on archival ROSAT data. These surveys differ operationally in two main ways: (1) in the source detection algorithm, including the method by which sources are classified as extended; and (2) in the optical follow-up carried out, specifically the design of the imaging program.

As already mentioned, in WARPS we replaced the standard sliding box detection algorithm, which has difficulties detecting extended sources of low surface brightness, with the VTP algorithm (§ 2.1). VTP is one of several such algorithms currently in use for the detection of clusters in archival X-ray data. Three of the others are based on wavelet techniques (in particular those used by the RDCS, SHARC-Bright and CfA 160 deg<sup>2</sup> teams), while another is based on modifying the sliding box algorithm with smoothing and wavelet transforms (the SHARC-south survey, Collins et al. 1997). At least in theory, both VTP and wavelet techniques should be equally sensitive to surface brightness enhancements, regardless of their extent or morphology.

While the basic outlines of the optical follow-up program for each survey are similar, some important differences exist. Chief among these are the following. (1) WARPS is the only survey which performed optical imaging on sources which were not flagged as possibly extended by its detection algorithm (see § 2.3.1). (2) RDCS is the only survey that has included near-infrared imaging in its follow-up program. (3) SHARC-Bright is the only survey that used a completely automated ‘friends-of-friends’ analysis to screen for possibly blended X-ray sources. Each of these could conceivably have an impact on the completeness and content of the respective samples.

A comparison of the number counts as well as the results in overlapping fields is useful in judging the efficacy of each procedure, and the completeness of each sample. The efficacy of a detection algorithm in detecting extended sources can be judged in several ways. The first is to compare the number of sources that were extended by eye in a given field with the number of extended sources found by the detection algorithm. This is what might be called the “false negative” detection rate. For WARPS, such a visual inspection was done for every field as a part of the deblending process detailed in Paper I. These inspections were originally done as part of an effort to distinguish blends of two or more point sources from truly

extended X-ray sources, but they also have the side benefit of being able to find extended sources which may have been missed by VTP. This visual examination yielded only one more possibly extended source, listed multiply as WARPJ1414.9+1120, WARPJ1415.0+1119 and WARPJ1415.2+1119, compared to over 30 extended sources. It should be noted that this source *was* found by running VTP at the lowest of the three thresholds described in Paper I, but was removed by the deblending process that paper described, and manually returned to the catalog after our by-eye inspections. It is also not surprising that this source is extremely faint and in fact does not make our flux-limited sample (§ 4). This very low fraction of “lost” sources gives us considerable confidence in the reliability of VTP for detecting all extended and point sources up to our selected flux limit (for a discussion of the statistical significance of this flux limit see Paper I).

A second way to test the efficacy of our selection method, and in particular  $f_{ext}$ , described in § 2.1 and Paper I, is to look at the relationship between the fraction of truly extended X-ray sources (i.e., clusters, elliptical galaxies, etc.) and  $f_{ext}$ . In Figure 1d we show a histogram of the fraction of sources identified as clusters, as a function of  $f_{ext}$ . As can be seen, one of the clusters in our flux-limited sample has  $f_{ext} < 1.1$  (WARPJ2302.8+0843), and two more likely clusters with  $f_{ext} < 1$  fall below the limit (WARPJ1537.7+1201 and WARPJ1501.0–0824, which are in high-background fields). These clusters were identified only because our optical follow-up program included not only all possibly extended sources, but also sources flagged as not extended by VTP, that might be associated with visible galaxies or were blank fields. The cluster fraction increases markedly at higher values: 11% of sources with  $1.1 < f_{ext} < 1.2$  are clusters, but about 47% of sources with  $f_{ext} > 1.2$  are clusters. A similar fraction holds at higher extents. The fact that it never approaches unity attests to the fact that a significant number of X-ray blends are present. This pattern gives us further confidence in the efficacy of VTP as a method to detect extended sources.

It is not surprising that two of three clusters with  $f_{ext} < 1.1$  are among our faintest and most distant. Simulations by Evrard & Henry (1991) showed that cosmological  $(1+z)^{-4}$  surface brightness dimming can cause a cluster to appear as a point source at high  $z$ . Those authors predicted that ROSAT would begin to have trouble distinguishing extended X-ray emission in clusters from point-like sources, at redshifts  $z > 0.4$ . The results of this and other X-ray surveys for clusters of galaxies (Papers I, II; Romer et al. 2000; Collins et al. 1997; Rosati et al. 1998; Vikhlinin et al. 1998b) have shown that this prediction was too pessimistic, perhaps partly due to evolution of the spatial and/or spectral distribution of the ICM in clusters with redshift (which is predicted in hierarchical models of structure formation; see Bahcall & Cen 1992; Viana & Liddle 1996), or the presence of substructure and less centrally concentrated emission. However, at particularly high redshifts this effect should not be forgotten and may be a cause of incompleteness not only in our survey but in

all ROSAT-based surveys (see also the simulations by Adami et al. 2000).

The third and final way to test efficacy is to compare the overall number counts in WARPS with those of other surveys. If indeed all of the methods being employed are comparably effective in finding extended X-ray sources and hence clusters, we should find comparable log N - log S distributions. Rosati et al. (1998) have already addressed this issue regarding the comparison of WARPS-I with RDCS: despite the fact that RDCS has found a few clusters at  $z > 1$  (Rosati et al. 2000), the overall number counts are comparable. The situation is similar for the 160 deg<sup>2</sup> survey of Vikhlinin et al. (1998b), which has a log N - log S distribution similar to WARPS-I (Vikhlinin et al. 1998b, their Fig. 10). Moreover, since that survey has published its catalog we can cross-check the sources and IDs in the fields that are in common between the two. A total of 20 ROSAT fields are common to WARPS and 160 deg<sup>2</sup> survey, and the sources and IDs agree well (in particular the cluster IDs are in complete agreement in the overlapping regimes of flux and detector area, and the fluxes also agree well, with a mean ratio of VMF/WARPS=0.98 ± 0.26). The sources in common are noted in Table 3. Finally comparing the number counts of WARPS-I and SHARC-south (Collins et al. 1997; Burke et al. 1997) we see that the two curves are also comparable.

Some similar comparisons can also be made with the SHARC-Bright survey (Romer et al. 2000; Adami et al. 2000), which however have not published a log N - log S distribution. Comparing our field list with that of SHARC-Bright (Romer et al. 2000) we find 60 fields in common. WARPS finds all 6 of the clusters found by SHARC-Bright in those fields (down to the SHARC-Bright flux limit), as well as two not found by SHARC-Bright: WARPJ1552.2+2013 and WARPJ0238.0–5224. The overall number counts also do not agree: SHARC-Bright find 37 clusters with fluxes  $F_x \gtrsim 2.8 \times 10^{-13}$  erg cm<sup>-2</sup> s<sup>-1</sup> (as explained in Romer et al. 2000, this limit is approximate because they perform their limit calculation in counts, rather than flux), in a total area of 178.6 deg<sup>2</sup>. By comparison, our published log N - log S distribution (Paper II) predicts  $57 \pm 8$  clusters within the SHARC-Bright survey - i.e., the number counts for SHARC-Bright are too low compared with the WARPS-I, SHARC-S, RDCS and CfA 160 deg<sup>2</sup> surveys, at the 2.5  $\sigma$  level.

A similar difference in number counts is found when comparing the extended source lists of the CfA 160 deg<sup>2</sup> and SHARC-Bright surveys. Romer et al. (2000, see their §7.5) note that SHARC-Bright finds only 13 of 21 CfA 160 deg<sup>2</sup> clusters that are both within the SHARC-Bright survey area and above the SHARC-Bright flux limit. This is consistent with the above comparison of the WARPS-I log N - log S with the total number of galaxies from SHARC-Bright. Of the 8 CfA 160 deg<sup>2</sup> clusters missed by SHARC-Bright, 7 did not meet the SHARC-Bright “filling factor” criterion (essentially an automated friends of friends analysis intended to spot blends), while 1 did not meet their extent criterion. Thus a comparison to

both our results and that of the CfA 160 deg<sup>2</sup> results suggests either serious incompleteness, or systematic miscalculation of cluster fluxes by SHARC-Bright.

Romer et al. (2000) have addressed this last point by comparing the fluxes for sources in common between SHARC-Bright and the CfA 160 deg<sup>2</sup>. They find that SHARC-Bright find systematically higher fluxes than the 160 deg<sup>2</sup> survey, with a mean ratio SHARC-B/VMF =  $1.18 \pm 0.26$ , and attribute the difference to assuming a fixed core radius of 250 kpc (when the Vikhlinin et al. 1998b core radius values are used the systematic difference disappears). We find a similar average ratio SHARC-B/WARPS =  $1.37 \pm 0.26$  but we are unable to test whether this would be removed by using the SHARC-Bright pipeline with our core radii.

If the SHARC-Bright fluxes are indeed at 20-30% variance with other, equivalent, surveys, this would bring their overall number counts into agreement with those of WARPS-I and the CfA 160 deg<sup>2</sup>. However this still does not explain why SHARC-Bright appears to miss  $\sim 30 - 40\%$  of clusters which should meet their flux limit. Romer et al. (2000) conclude that this “illustrates how differing selection criteria produce differing cluster samples and that detailed simulations are required to determine a survey’s selection function.” These were done in Adami et al. (2000), which simulated the selection function by placing cluster sources of various X-ray morphology randomly in real PSPC data, and then tracking the extended source finding rate. But Adami et al. (2000) do not test explicitly the filling factor criterion which appears to have been responsible for SHARC-Bright missing fully 1/3 of the clusters within their survey area. By placing simulated clusters randomly in real PSPC data, Adami et al. (2000) do *implicitly* test the filling factor criterion, but they compile no statistics regarding *e.g.*, the nearness of the simulated cluster to other sources in each field. The Adami et al. (2000) simulations result in a selection function which brings the SHARC-Bright X-ray luminosity function into agreement with the results found by RDCS, WARPS and other surveys. However, the lack of an explicit test of the filling factor criterion makes their result more uncertain.

Because of the exhaustive nature of the WARPS optical follow-up program (§ 2.3), we can make one further comment. Unlike all the other surveys WARPS investigated thoroughly all possible cluster sources, even if the source was not extended according to the VTP algorithm. All other ROSAT based surveys did not image optically any sources that were not found to be extended by their source detection algorithm. The similarity of the WARPS, SHARC-south, RDCS and 160 deg<sup>2</sup> number counts, plus the fact that we only found one cluster in our complete sample among the sources we flagged as not extended, assures us that for our sample as well as the RDCS and CfA 160 deg<sup>2</sup> this effect is negligible overall, but may not be insignificant at the highest redshifts, although the size of the effect depends on the details of the algorithm used. However, the utility of this practice becomes clear in the

comparison with SHARC-Bright (above), since the careful evaluation of questionable sources and followup optical observations of those sources might have enabled them to identify the missing 30-40% of *bona fide*, X-ray bright clusters within their survey area and flux limits.

## 4. Clusters of Galaxies

### 4.1. The Cluster Catalog

In Table 4 we have listed all 22 members of the statistically complete WARPS-I cluster sample. Similarly, in Table 5 we list 13 additional clusters and 3 possible other clusters. Individual descriptions of all the sources are given in § 4.4. The columns in Table 4 and Table 5 are as follows:

1. The assigned cluster name.
2. The right ascension (hours, minutes, seconds) in J2000 coordinates, as extracted from the ROSAT data.
3. The declination (degrees, minutes, seconds) in J2000 coordinates, as extracted from the ROSAT data.
4. The extent parameter  $f_{ext}$  as discussed in § 2.1.
5. The hydrogen column density from Dickey & Lockman (1990) in units of  $10^{20} \text{ cm}^{-2}$ .
6. The unabsorbed source flux in units of  $10^{-13} \text{ ergs cm}^{-2} \text{ s}^{-1}$  in the 0.5–2.0 keV band as described in § 2.1. For some clusters this flux may include a component from contaminating sources (e.g., AGN). See § 4.4 for details for each cluster.
7. The rest-frame source luminosity in units of  $10^{44} \text{ ergs s}^{-1}$  in the 0.5–2.0 keV band derived in the same manner as the flux. Values of  $q_0 = 0.5$  and  $H_0 = 50 \text{ km s}^{-1} \text{ Mpc}^{-1}$  were assumed.
8. The core radius of the cluster in arcseconds. Note that this is very crude as it is based on ROSAT data which in most cases barely resolve the cluster.
9. The redshift of the cluster.
10. The number of galaxy redshifts used to derive the cluster redshift.



11. Flags. A “c” indicate that the cluster is contaminated or possibly contaminated by other sources. In Table 5, a “<” indicates that the cluster flux falls below the limit for inclusion in the statistically complete, flux-limited sample. An “?” indicates a possible cluster or group for which optical follow-up was not completed, usually because it was below the flux limit. An “8” indicates that the cluster was found in a field targeted at another cluster while an “b” indicates that this field was dropped due to high background. See the notes in § 4.4 for flagged sources.
12. Alternate names or notes. The same as for Table 2.

In Figure 3 we show the optical images we obtained of these clusters, with the X-ray emission contours overlaid. These images, as well as other information, are also available on our WWW site.

## 4.2. Radio Sources

In Table 6, we list the position, positional error, distance from the x-ray centroid, and flux of all radio sources within  $2'$  of the X-ray centroid of each of these clusters, along with information regarding the possible nature of the radio sources (see also § 2.2.2). In each case we have checked to see whether some fraction of the X-ray emission could come from the radio source, and make comments to this effect in § 4.4.

## 4.3. The Statistically Complete WARPS-I Sample

We have selected from the sources identified as clusters a statistically complete, X-ray surface brightness limited sample of 22 clusters. This sample is somewhat different from the sample used to derive the  $\log N - \log S$  in Paper II. To make the WARPS-I sample consistent with that from WARPS-II, the PSPC field selection criteria for the statistical sample were made more restrictive (see § 2), and all the fields were reprocessed by VTP. The VTP algorithm was improved and refined between the WARPS-I and WARPS-II processing. This has changed the fluxes and extents slightly, by 5-10%, for some sources. A few clusters used in Paper II now fall below the flux limit (while others are now above it). However, these changes do not affect the conclusions of Paper II.

Figure 4 shows a histogram of the redshift distribution of the sample. As can be seen, the clusters in the WARPS-I sample range in redshift from  $z = 0.06 - 0.75$  (see also Table 4).

#### 4.4. Descriptions of Individual Clusters

Here we provide detailed information about clusters in both the statistical and supplemental samples. See Figure 3 for optical CCD images with X-ray emission contours overlaid. In this section, SHARC-B refers to the SHARC Bright Survey catalog (Romer et al. 2000), VMF to the CfA 160 deg<sup>2</sup> survey (Vikhlinin et al. 1998b), and RIXOS to the RIXOS survey catalog (Mason et al. 2000).

**WARPJ0022.0+0422** This extended X-ray source is associated with a cluster, GH000190.5+0405 (no previous redshift), which was previously discovered by Gunn et al. (1986). An HRI observation of this field failed to detect the cluster, but it is near the edge of the HRI field-of-view. The northeastern X-ray component is identified with an AGN at  $z = 0.272$ , unrelated to the cluster. Aperture photometry on the PSPC image suggests that the quoted flux includes a  $\approx 25\%$  contribution from the AGN. This cluster is in a ROSAT field targeted at another cluster (GH0 0020+0407 at  $z=0.698$ ) and so is not part of the statistically complete sample.

**WARPJ0023.1+0421** This X-ray source originates in a poor cluster of galaxies at  $z = 0.453$ . An HRI observation of this field shows a marginal detection of an extended source. All the 7 galaxies for which spectra were obtained, including the 3 cluster members, show evidence of narrow emission lines. The brightest cluster member, offset from the X-ray peak, has O II emission and strong H $\delta$  absorption, indicative of recent star formation activity. The cluster galaxy at the X-ray peak has strong O II and weaker H $\beta$  and O III emission, indicative of a cooling flow or LINER-type spectrum rather than a Seyfert 2. This cluster is in a ROSAT field targeted at another cluster (GH0 0020+0407 at  $z=0.698$ ) and so is not part of the statistically complete sample.

**WARPJ0111.6–3811** The galaxies associated with this X-ray source appear to fall into two regions: a northern cluster at  $z = 0.121$  ( $n_z = 3$ ) and a south western one at  $z = 0.132$  ( $n_z = 4$ ). The x-ray emission originates predominantly from the northern cluster (the southern cluster clearly falls well below our flux limit). The VTP flux estimate excludes the southern cluster and the bright point-like X-ray source to the southeast, which is identified with a QSO at  $z = 0.894$ .

**WARPJ0144.5+0212** This clearly extended X-ray source corresponds with the position of a poor cluster of galaxies at  $z = 0.165$ , revealed by the optical image (Figure 3). The extended nature of the X-ray emission and the position of the BCG coincident with the X-ray peak makes it clear that the majority of the X-ray emission comes from the cluster, but the presence of an 80 mJy radio source (Table 6) makes some

caution advisable. The radio source corresponds to one of the fainter galaxies very near the BCG, which may be a background radio galaxy or other AGN. However, we see no evidence for X-ray point-like emission at this position so the possible contribution from the radio source is small. A second, much fainter, radio source is located in this cluster’s outskirts. The quoted flux includes both northern and southern X-ray components.

**WARPJ0206.3+1511** Our redshift is from two galaxies but agrees with the redshift in the RIXOS catalog and the estimate in the VMF catalog. The quoted X-ray flux may include a small contribution from a bright star to the east of the cluster.

**WARPJ0210.2–3932** The cluster was discovered during the reprocessing and corresponds to VMF 24. VMF estimate a photometric redshift of  $z = 0.19$ . Since it is well below our flux limit, no spectroscopic follow-up was done.

**WARPJ0210.4–3929** Our redshift for this cluster ( $z = 0.273$ ) is tentative, being based on low signal to noise observations at the CTIO 1.5m and at the AAT in service time. In both instances, spectra were taken of the two galaxies near the X-ray centroid. Those spectra show a continuum break at about  $5000 \text{ \AA}$  in both galaxies and probable CaII at  $4994/5059 \text{ \AA}$  and  $H\beta$  at  $6203 \text{ \AA}$  in the brighter galaxy only. This cluster is also in the VMF catalog, who estimate a photometric redshift of  $z = 0.27$  with a range of 0.20-0.30. Further spectroscopic observations are required to confirm the redshift of this cluster.

**WARPJ0216.5–1747** This clearly extended X-ray source corresponds to the position of the optical cluster shown in Figure 3. Also in the X-ray error circle (and near X-ray peaks) are 2 M stars. A 7.2 mJy radio source (Table 6) is about  $100''$  north of the X-ray centroid (and well outside the X-ray emission contours) which is associated with a foreground 14th magnitude galaxy. The X-ray image shows no sign of point source contamination, and we estimate that  $<30\%$  of the PSPC flux is from the M stars, consistent with the  $\alpha_{ox}$  of M stars in Stocke et al. (1991).

**WARPJ0228.1–1005** This clearly extended X-ray source is associated with a cluster which is dominated by two bright galaxies that overlap on the sky. We only have a redshift ( $z = 0.149$ ) for one of them. The spectrum of the other galaxy contains only very weak absorption lines, and may possibly be a BL Lac object. It is also a faint radio source (7 mJy, Table 6). The HRI image confirms the cluster to be an extended X-ray source and also shows an unrelated point X-ray source  $\approx 1'$  to the northwest of the cluster. The quoted PSPC flux includes a  $\approx 10\%$  contribution from this source.

**WARPJ0234.2–0356** This distant ( $z = 0.447$ ) cluster falls just below the flux limit of our sample at  $6.4 \times 10^{-14}$  ergs cm $^{-2}$  s $^{-1}$ . The X-ray contours and the galaxy velocities (although from only 5 cluster members) suggest that the cluster has two components. The BCG of the northern component has narrow O II, O III and H $\alpha$  emission lines, as well as strong H $\delta$  absorption, perhaps indicating recent star-formation activity. It may be interacting with a nearby galaxy.

**WARPJ0238.0–5224** This massively extended X-ray source corresponds with the cluster Abell 3038. This source is also in the VMF and SHARC-B catalogs, but only in one of two fields within which the cluster is actually found (see § 3. We used the redshift from (Nesci & Altamore 1990), which has been confirmed by SHARC. An HRI image confirms the lack of point-source contamination.

**WARPJ0250.0+1908** We have only poor quality optical images of this source and two redshifts. However, this source is also in the SHARC-B catalog, who list a similar redshift ( $z = 0.12$ ). The northern X-ray source, visible on the contours, is excluded from the quoted X-ray flux.

**WARPJ0255.3+0004** This marginally extended source was imaged with the WIYN 3.5m revealing a possible distant group or poor cluster, but as it was below the flux limit, no further follow-up was done.

**WARPJ0348.1–1201** This extended X-ray source emanates from the unrelaxed  $z = 0.4876$  cluster shown in the optical image. The brightest galaxies in this cluster fall along a southeast to northwest line. One of these is a 34 mJy radio source (Table 6), but no X-ray point-like emission is evident near the position of this radio source.

**WARPJ0951.7–0128** This clearly extended X-ray source is associated with a  $z = 0.567$  cluster of galaxies. Our redshift agrees very well with the photometric estimate published in the VMF catalog. Our cross-correlations with the NVSS and FIRST revealed a 6.2 mJy radio source near the X-ray centroid (Table 6). The optical counterpart to this radio source is a 20th magnitude galaxy, likely a cluster member. We see some evidence for unresolved X-ray emission near this position, so some of the X-ray emission may originate from the radio source. We have only one firm redshift for this cluster and one other probable similar redshift.

**WARPJ1113.0–2615** The galaxies close to the brightest galaxy in this distant ( $z = 0.725$ ) cluster show morphological evidence for interactions, and perhaps a gravitationally lensed arc. The X-ray source is clearly extended but low surface brightness and is very close to the flux limit for our statistically complete sample. Based on visual inspection

of our deblending results, we have used the count rate at threshold 3 (rather than 4) for this object.

**WARPJ1406.2+2830** We obtained only a poor image and one low quality redshift of  $z = 0.552$  for the BCG of this source. This source is also listed in the CRSS survey (Boyle, Wilkes, & Elvis 1997), but as a galaxy only; the CRSS give a redshift of 0.546, also based on a low quality spectrum. VMF list this source with the CRSS redshift, but also identify the source as a cluster. We observed this cluster with the HRI in 1996, with exposure time 19900 seconds, but the HRI failed to detect extended emission from the cluster or any point source contamination. Given the lower sensitivity of the HRI compared to the PSPC to low surface brightness X-ray emission, this result supports the assertion that this X-ray source is indeed extended.

**WARPJ1406.9+2834** An HRI image shows an extended source at the position of the cluster plus a point X-ray source  $90''$  east of the cluster center. The flux quoted includes the flux from the point source, but analysis of the HRI image indicates that the point-source flux is at most 25% of the cluster flux. This source is also in the VMF and SHARC catalogs.

**WARPJ1407.6+3415** This extended X-ray source falls somewhat below our statistically complete sample's flux limit. We have one low quality redshift at  $z = 0.577$  and another at  $z = 0.3793$ , which contains narrow emission lines (O II equivalent width is  $20\text{\AA}$ ). This may be a cluster contaminated by a foreground star-forming galaxy or LINER. No further follow-up was done.

**WARPJ1415.1+3612** This distant cluster contains a 5.4 mJy radio source near the center of the X-ray contours possibly associated with the cluster BCG. The X-ray morphology indicates possible point-source contamination. We have obtained optical spectroscopy of this cluster with Keck but the data are noisy and we have been unable to extract a redshift.

**WARPJ1415.3+2308** This poor cluster, the lowest redshift cluster in the sample at  $z = 0.064$ , is dominated by two bright, probably interacting, galaxies. One of these galaxies has strong narrow  $H\alpha$  emission and may contain a low luminosity AGN. An 8.7 mJy radio source is also present in the cluster center and coincides with one of the bright central galaxies. The X-ray morphology, although from a low signal-to-noise image, may indicate some point-source contamination from within the cluster, as well as extended emission. This cluster has been omitted from the statistically complete sample since it is in a ROSAT field targeted at another galaxy cluster.

**WARPJ1416.4+2315** This extended X-ray source originates in a  $z = 0.135$  cluster of galaxies visible on both the sky survey plate and the deeper image. A 4.1 mJy radio source (Table 6) appears to be associated with the BCG. Two of the three galaxies with redshifts (but not the BCG) show strong narrow  $H\alpha$  emission, and one may be associated with weak X-ray emission. The X-ray flux from a QSO (HS1414+2330) behind the cluster also contributes to the quoted flux at about the 25% level according to the WGACAT, (White et al. 1995), but both of these sources are weak contaminants compared to the bright extended cluster emission. This a candidate for being a ‘fossil’ group or cluster of galaxies. This cluster has been omitted from the statistically complete sample since it is in a field targeted at another galaxy cluster.

**WARPJ1418.5+2511** This massively extended, luminous ( $L_{X,bol} \sim 10^{45}$  erg s $^{-1}$ ) X-ray source originates in a  $z = 0.29$  cluster of galaxies which can be seen both on the sky survey plate and the KPNO image. Our cross-correlation with the NVSS reveals a 38.9 mJy radio source 65'' from the X-ray centroid (Table 6), which is associated with a likely cluster member. We see no X-ray enhancement at the position of the radio source, so it is unlikely to contribute a major fraction of the X-ray emission. The FIRST image reveals that this radio source may have a wide-angle-tail morphology, which is not at all atypical of cluster radio galaxies (e.g., Ledlow & Owen 1995), although such sources are more commonly found in cluster cores. The Butcher-Oemler properties of this cluster have been studied by Fairley et al. (2001). The cluster has been previously discussed by Stocke et al. (1983) and other authors, as part of the Einstein Observatory Medium Sensitivity Survey (MSS, but note that this source is not in the later EMSS), and by Nandra et al. (1993) (it is only  $\approx 8'$  from the bright Seyfert 1 galaxy NGC 5548).

**WARPJ1501.0–0824** This is one of two point-like X-ray sources identified by our optical imaging program as a likely cluster of galaxies. We have not obtained optical spectroscopy since its X-ray flux is below the limit for our statistically complete sample. Aperture photometry of the BCG yields  $R = 19.54 \pm 0.3$ , which corresponds to a redshift estimate of  $z = 0.51 \pm 0.07$  using the photometric estimation method of Vikhlinin et al. (1998b). Our cross-correlation with the NVSS (Table 6) finds a resolved radio source 23'' from the X-ray source, which appears to be associated with a likely cluster galaxy. This indicates possible emission from an AGN; however, the radio position is well outside the X-ray position’s error circle, and in addition the position of the radio source is well away from the optical center of the cluster. The field was later removed from consideration in the statistically complete sample due to its high background.

**WARPJ1515.5+4346** This cluster was included as part of a larger extremely diffuse

source which was later resolved into three groupings. The northern clump (now WARPJ1515.7+4352) appears point-like and spectroscopy reveals a broad-lined AGN at  $z = 0.524$ . The southern clump is WARPJ1515.5+4346 at  $z = 0.135$  ( $n_z = 3$ ) but is just outside the  $15'$  radius from the ROSAT field center. The identification of the central source is uncertain. It may be a cluster with a redshift  $z = 0.136$  ( $n_z = 1$ ) or  $z = 0.237$  ( $n_z = 2$ ). By itself, the central source is below our count rate cutoff. Even if it is associated with WARPJ1515.5+4346, the centroid of the emission is still outside of the  $15'$  radius. Therefore, the cluster is not part of the statistically complete sample. This source corresponds to VMF 169, which has a listed position about  $4'$  north, suggesting that the VMF source includes more of the diffuse emission.

**WARPJ1517.9+3127** This distant ( $z = 0.744$ ,  $n_z = 2$ ), but luminous, cluster is just below our completeness threshold. In later reprocessing with an updated VTP it failed to even make the count rate cutoff. Therefore, it is not part of the statistically complete sample.

**WARPJ1537.7+1201** This X-ray source is associated with a group or poor cluster at  $z = 0.136$ . It has two X-ray emission components, which appear to be centered around the positions of the two brightest galaxies. This source was decomposed into two components and was manually reinserted following inspection of the X-ray photon distribution for the field. The source is in a ROSAT field with high background and so the cluster has been excluded from our statistically complete sample.

**WARPJ1552.2+2013** One of the member galaxies, located at a minor peak in the X-ray surface brightness, has narrow, and possibly broad,  $H\alpha$  emission. However, any contamination to the X-ray luminosity is at a small level. This system is a candidate ‘fossil’ group or poor cluster.

**WARPJ2038.4–0125** This extended X-ray source originates in one of the most distant ( $z = 0.679$ ) clusters of galaxies in the WARPS-I sample. Two radio sources are located in the field which may be associated with cluster galaxies (Table 6), but these are both well away from the X-ray emission contours.

**WARPJ2108.6–0507** This extended X-ray source is associated with a  $z = 0.222$  cluster which can be seen on both the sky survey plate and image. A faint (3.7 mJy; Table 6) radio source is located near the X-ray centroid, which does not appear to be associated with any of the brighter cluster galaxies as it is in a blank field according to our image. The X-ray morphology is compact; there may be a cooling flow or point-source contamination, although none of the optical spectra for three objects in the cluster core suggest that they are the counterparts.

**WARPJ2108.7–0516** This extended X-ray source is associated with a  $z = 0.317$  cluster of galaxies. A 9.6 mJy radio source (Table 6) located  $41''$  from the X-ray centroid, which does not correspond to the optical position of any galaxy visible on the CFHT image. We have 10 spectroscopically confirmed galaxy members. The cluster has at least two components, both in X-ray morphology and galaxy velocities. The x-ray source to the east is included in the quoted flux, but whether it is related to the cluster is not clear.

**WARPJ2146.0+0423** This massively extended X-ray source is associated with a  $z = 0.5324$  cluster of galaxies. Our cross-correlation with the NVSS (Table 6) reveals an unresolved radio source  $30''$  from the X-ray centroid. A likely cluster member is within the radio error circle, but the overlay of the optical and X-ray images does not indicate any enhancement of the X-ray emission near its position. The source extent and lack of point source contamination is confirmed by an HRI observation. This cluster is also in the Gunn et al. (1986) (GHO) sample. Oke (private communication) confirms the cluster redshift as  $z = 0.53$  (from 2 redshifts) and also finds two (emission line) galaxies at  $z=0.40$ , suggesting a superposed foreground cluster may exist. The Butcher-Oemler properties of this cluster have been studied by Fairley et al. (2001), who also find evidence for a foreground group. We have assumed all the X-ray flux originates in the  $z = 0.532$  system, since the X-ray emission is centered on the BCG of this system. A small fraction of the quoted X-ray flux may arise in the bright nearby elliptical galaxy visible in the overlay.

**WARPJ2239.4–0547, WARPJ2239.6–0543** These two sources were found to be associated with the cluster Abell 2465. The PSPC image shows two clearly extended X-ray sources, each centered on a well-defined cluster core. We have obtained optical spectroscopy of objects in both clusters, which confirms them to be at slightly different redshifts ( $z = 0.2419$  versus  $z = 0.2427$  for six galaxies apiece). We believe that these clusters may be in the process of merging. The brightest galaxy of WARPJ2239.6-0543 is also an 8.4 mJy radio source. However, the morphology in an HRI image does not reveal any point source emission, and none of the optical spectra of galaxies in the cluster core show emission lines.

**WARPJ2239.5–0600** This X-ray source is associated with a compact group at  $z = 0.174$ , and it falls just below the threshold for inclusion in our statistically complete sample at a flux of  $6.30 \times 10^{-14}$  ergs cm $^{-2}$  s $^{-1}$ .

**WARPJ2302.8+0843** Keck imaging and spectroscopy of this distant cluster ( $z = 0.722, n_z = 1$ ) indicate that it may be contaminated by a BL Lac. This is supported by the presence of a 25 mJy radio source very close to the cluster center. The level of contamination is impossible to tell from the low signal-to-noise PSPC image. A recent image of this



source with *Chandra* shows that the X-ray emission is entirely extended, however (we will report on this image in a future paper).

**WARPJ2319.5+1226** We have only a good redshift for the BCG of this poor cluster or group ( $z = 0.125$ ) and have chosen to use the RIXOS value of  $z=0.124$  ( $n_z = 3$ ).

**WARPJ2320.7+1659** This clearly extended X-ray source is associated with a  $z = 0.499$  cluster of galaxies and a  $z = 1.81$  QSO at the x-ray peak. Most of the flux may be from the QSO, but the level of contamination is impossible to tell from the low signal-to-noise PSPC image. However, since the total flux is just above our flux limit, any small contribution from the QSO would reduce the cluster flux to a level below the flux limit, so we have excluded this source from our statistically complete sample. Our cross-correlation with the NVSS (Table 6) also reveals a 2.8 mJy radio source  $41''$  from the X-ray centroid, but no obvious X-ray enhancement is visible at this position.

## 5. Discussion and Future Prospects

Here we have presented the identifications and cluster catalogs from the first phase of the WARPS project, an extensive survey of deep ROSAT pointings using a surface brightness sensitive algorithm. In doing so, we have also presented some comparisons of the results of WARPS-I to other cluster surveys, which help place the the various cluster detection algorithms and follow-up programs in perspective. As can be seen, the findings of WARPS are largely similar to those of other cluster surveys as regards the space density of X-ray emitting clusters.

The number of serendipitous X-ray surveys for clusters of galaxies now number more than a dozen. For example, the list of those based on ROSAT data includes BCS (Ebeling et al. 1998, 1997, 2000), WARPS (Papers I, II), RDCS (Rosati et al. 1998), SHARC-Bright (Romer et al. 2000), SHARC-south (Burke et al. 1997; Collins et al. 1997), CfA 160 deg<sup>2</sup> (Vikhlinin et al. 1998b), NEP (Gioia et al. 2001), NORAS (Böhringer et al. 2000), REFLEX (Boehringer et al. 2001), MACS (Ebeling et al. 2001c) and CIZA (Ebeling, Mullis, & Tully 2001). Each of these surveys use different selection criteria and/or X-ray source-detection algorithms, but largely similar optical follow-up programs. Meanwhile, several optical surveys have used moderate depth, large-area images of the sky combined with algorithms that measure overdensities of galaxies (e.g., PDCS, Lubin 1995; Postman et al. 1996; RCS, Gladders & Yee 2000). All of these surveys represent a fertile ground for constraining cosmological parameters as well as learning more about appropriate methods for finding massive clusters of galaxies and their attendant selection effects. However, precious few efforts (most notably

ROXS, Donahue et al. 2000) are underway to understand the relationship of the selection effects in optical and X-ray surveys.

Despite the different emphases inherent in each method, all of the new surveys show no evidence for evolution at all but the most X-ray luminous clusters of galaxies at redshifts up to  $z = 0.8$ . The X-ray luminosity-temperature relationship (Paper IV, Mushotzky & Scharf 1997) at  $z < 0.8$ , also shows no sign of evolution. Yet at  $z \sim 1$ , there are tantalizing hints of evolution in the cluster population. This evidence includes a preponderance of irregular X-ray morphologies, optical cluster galaxy distributions and colors (Paper III, Stanford et al. 2001, although see Paper V for a notable counter-example), as well as a suggestion that the space density of the most luminous ( $L_X > 5 \times 10^{44}$  erg s $^{-1}$ ) clusters decreases significantly at redshifts  $z > 0.5$  (Rosati et al. 1998; Vikhlinin et al. 1998a; although for a counterargument see Paper V). Taken together, these lines of evidence might suggest that the epoch of cluster formation is currently just out of reach of our current observational tools, which are limited to finding clusters at  $z < 1.25$  by the limitations inherent in observing in the optical (at  $z = 1.25$  the Ca break passes out of the I band), even though simulations (*e.g.*, Paper I) show an ability to detect X-ray luminous, extended sources at redshifts up to nearly  $z = 2$ .

This presents future X-ray surveys (*e.g.*, *Chandra* or XMM-Newton) with significant challenges, since one would expect them to contain large numbers of  $z > 1$  clusters. Indeed, as we pointed out in Papers III and V, WARPS is sensitive enough to include clusters of  $L_X \sim 10^{45}$  erg s $^{-1}$  out to redshifts of nearly 2. Even given the highly unclear (and very poorly explored) state of galaxy evolution at  $z \gtrsim 1$ , it is obvious from the current literature that, at  $z \sim 0.8$ , the space density and ICM characteristics of clusters of galaxies show little difference from those observed at lower redshifts. It is therefore imperative that future surveys for clusters of galaxies include near-infrared observations, which should increase their window of sensitivity for identifying cluster counterparts to X-ray sources out to  $z \sim 4.5$  (*i.e.*, when the H & K break passes out of the K band). Of the current X-ray surveys, only RDCS has included near-infrared observations in its follow-up program, and as a result, RDCS is the only X-ray selected sample of clusters to contain  $z > 1$  objects (Rosati et al. 1999, 2000), albeit only a handful (4 according to Rosati et al. 2000 and P. Rosati, private communication from an incomplete survey of about 80% of RDCS blank-field X-ray sources).

The now overwhelming evidence of little or no significant evolution in the space density of clusters at redshifts up to 0.8 is difficult to reconcile with  $\Omega_m = 1$  cold dark matter cosmologies, which predict significant evolution in the cluster LF at  $z \gtrsim 0.3$ . However, as Bode et al. (2001) show, a great deal of degeneracy remains in the predictions of hierarchical models of structure formation at  $z > 1$ , and coincidentally, this is where the fewest such X-ray selected clusters are known. It is at these highest redshifts that future X-ray and

other surveys for clusters (notably Sunyaev-Zel’dovich effect methods, see Xue & Wu 2001) will have to concentrate their efforts and where they will have the most impact.

E. S. P. acknowledges support from *Chandra* grant SAO1800627. H. E. acknowledges support from NASA LTSA grant NAG5-8253. C. A. S. acknowledges support from NASA LTSA grant NAG5-3257 (PI: M. Donahue). L. R. J. acknowledges the support of the U. S. National Research Council and the UK PPARC. We acknowledge interesting conversations with and emails from P. Rosati, C. Norman, M. Donahue, J. P. Henry, J. T. Stocke, R. Mushotzky, M. Henriksen, A. Evrard and B. Mathiesen.

The WARPS team acknowledges the long-term support of many different time allocation committees, including those at Kitt Peak National Observatory, Cerro Tololo Inter-American Observatory and the University of Hawaii, for the observations detailed in this paper. Part of the observations used in this paper were obtained at the MDM Observatory on Kitt Peak in Arizona. Some of the data presented herein were obtained at the W.M. Keck Observatory, which is operated as a scientific partnership among the California Institute of Technology, the University of California and the National Aeronautics and Space Administration. The Keck Observatory was made possible by the generous financial support of the W.M. Keck Foundation. This research has made use of data obtained through the High Energy Astrophysics Science Archive Research Center Online Service, provided by the NASA/Goddard Space Flight Center. This research has made use of the NASA/IPAC Extragalactic Database (NED) which is operated by the Jet Propulsion Laboratory, California Institute of Technology, under contract with the National Aeronautics and Space Administration. This research has also made use of the NRAO-VLA Sky Survey, which was carried out at the NRAO Very Large Array. NRAO is a facility of Associated Universities, Inc., and is a facility of the (USA) National Science Foundation. Finally, we wish to thank our referee, Dr. Luigi Guzzo, for helpful comments which improved considerably this paper.

## REFERENCES

- Adami, C., Ulmer, M. P., Romer, A. K., Nichol, R. C., Holden, B. P., & Pildis, R. A. 2000, *ApJS*, 131, 391
- Bahcall, N. A., & Cen, R. 1992, *ApJ*, 398, L81
- Becker, R. H., White, R. L., & Helfand, D. J. 1995, *ApJ*, 450, 559
- Bode, P., Bahcall, N. A., Ford, E. B., & Ostriker, J. P. 2001, *ApJ*, in press, astro-ph/0011376

- Boehringer, H., et al. 2001, A&A, submitted, astro-ph/0012266
- Böhringer, H., et al. 2000, ApJS, 129, 435
- Boyle, B. J., Wilkes, B. J., & Elvis, M., 1997, MNRAS, 285, 511
- Briel, U. G., & Pfeffermann, E. 1995, Proc. SPIE, 2518, 120
- Burke, D. J., Collins, C. A., Sharples, R. M., Romer, A. K., Holden, B. P., & Nichol, R. C. 1997, ApJ, 488, L83
- Carlberg, R. G., Morris, S. L., Yee, H. K. C., & Ellingson, E. 1997, ApJ, 479, L19
- Collins, C. A., Burke, D. J., Romer, A. K., Sharples, R. M., & Nichol, R. C. 1997, ApJ, 479, L117
- Condon, J. J., Cotton, W. D., Greisen, E. W., Yin, Q. F., Perley, R. A., Taylor, G. B., & Broderick, J. J. 1998, AJ, 115, 1693
- Dickey, J. M., & Lockman, F. J. 1990, ARA&A, 28, 215
- Donahue, M. E., Scharf, C., Mack, J., Lee, P., Postman, M., Dickinson, M., Rosati, P., & Stocke, J. 2000, in American Astronomical Society Meeting 197, #57.02, Vol. 197, 5702
- Ebeling, H. 1993, Ph.D. thesis, Ludwig-Maximilians-Universität München
- Ebeling, H., Edge, A. C., Böhringer, H., Allen, S. W., Crawford, C. S., Fabian, A. C., Voges, W., & Huchra, J. P. 1998, MNRAS, 301, 881
- Ebeling, H., Edge, A. C., Fabian, A. C., Allen, S. W., Crawford, C. S., & Böhringer, H. 1997, ApJ, 479, L101
- Ebeling, H., et al., 2000, MNRAS, 318, 333
- Ebeling, H., Edge, A. C., & Henry, J. P. 2001c, ApJ, 553, 668
- Ebeling, H., Jones, L. R., Fairley, B., Perlman, E., Scharf, C. A., & Horner, D. 2001a, ApJ, 548, L23 (Paper V)
- Ebeling, H., Mullis, C. R., Tully, R. B., 2001, ApJ, submitted
- Ebeling, H., et al. 2001b, ApJ, 534, 133 (Paper III)
- Ebeling, H., & Wiedenmann, G. 1993, Phys. Rev. E, 47, 704

- Edge, A. C., Stewart, G. C., Fabian, A. C., & Arnaud, K. A. 1990, MNRAS, 245, 559
- Ellingson, E., Green, R. F., & Yee, H. K. C. 1991, ApJ, 378, 476
- Evrard, A. E., & Henry, J. P. 1991, ApJ, 383, 95
- Fairley, B. W., Jones, L. R., Scharf, C., Ebeling, H., Perlman, E., Horner, D., Wegner, G., & Malkan, M. 2000, MNRAS, 315, 669 (Paper IV)
- Fairley, B., et al., 2001, in preparation
- Frenk, C. S., White, S. D. M., Efstathiou, G., & Davis, M. 1990, ApJ, 351, 10
- Gioia, I. M., Henry, J. P., Mullis, C. R., Voges, W., Briel, U. G., Böhringer, H., & Huchra, J. P., 2001, /apjl, in press, astro-ph/0102332
- Gladders, M. D., & Yee, H. K. C., 2000, AJ, 120, 2184
- Gunn, J. E., Hoessel, J. G., & Oke, J. B. 1986, ApJ, 306, 30
- Hardcastle, M. J., & Worrall, D. M. 1999, MNRAS, 309, 969
- Henry, J. P., Gioia, I. M., Maccacaro, T., Morris, S. L., Stocke, J. T., & Wolter, A. 1992, ApJ, 386, 408
- Horner, D. J., Mushotzky, R. F., & Scharf, C. A. 1999, ApJ, 520, 78
- Irwin, M., Maddox, S., & McMahon, R. 1994, Spectrum, 2, 14
- Jones, C., & Forman, W. 1984, ApJ, 276, 38
- Jones, L. R., Scharf, C., Ebeling, H., Perlman, E., Wegner, G., Malkan, M., & Horner, D. 1998, ApJ, 495, 100 (Paper II)
- Kaiser, N. 1991, ApJ, 383, 104
- Ledlow, M. J., & Owen, F. N. 1995, AJ, 109, 853
- Lubin, L. M., 1995, Ph. D. thesis, Princeton University
- Lucey, J. R. 1983, MNRAS, 204, 33
- Luppino, G. A., & Gioia, I. M. 1995, ApJ, 445, L77
- Mason, K. O., et al. 2000, MNRAS, 311, 456

- Mullis, C. R. 2000, in Large Scale Structure in the X-ray Universe, Proceedings of the 20-22 September 1999 Workshop, Santorini, Greece, eds. Plionis, M. & Georgantopoulos, I., Atlantisciences, Paris, France, p.149, 149
- Mushotzky, R. F., & Scharf, C. A. 1997, ApJ, 482, L13
- Nandra, K., et al. 1993, MNRAS, 260, 504
- Nesci, R., & Altamore, A., 1990, A&A, 234, 60
- Nichol, R. C., Holden, B. P., Romer, A. K., Ulmer, M. P., Burke, D. J., & Collins, C. A. 1997, ApJ, 481, 644
- Owen, F. N., & Ledlow, M. J. 1997, ApJS, 108, 41
- Postman, M., Lubin, L. M., Gunn, J. E., Oke, J. B., Hoessel, J. G., Schneider, D. P., Christensen, J. A., 1996, AJ, 111, 615
- Rector, T. A., Stocke, J. T., Perlman, E. S., & Gioia, I. M., 1999, ApJ, 516, 145.
- Romer, A. K., et al. 2000, ApJS, 126, 209
- Rosati, P., Borgani, S., della Ceca, R., Stanford, A., Eisenhardt, P., & Lidman, C. 2000, in Large Scale Structure in the X-ray Universe, Proceedings of the 20-22 September 1999 Workshop, Santorini, Greece, eds. Plionis, M. & Georgantopoulos, I., Atlantisciences, Paris, France, p.13, 13
- Rosati, P., Della Ceca, R., Norman, C., & Giacconi, R. 1998, ApJ, 492, L21
- Rosati, P., Stanford, S. A., Eisenhardt, P. R., Elston, R., Spinrad, H., Stern, D., & Dey, A. 1999, AJ, 118, 76
- Scharf, C. A., Jones, L. R., Ebeling, H., Perlman, E., Malkan, M., & Wegner, G. 1997, ApJ, 477, 79 (Paper I)
- Snowden, S. L., Plucinsky, P. P., Briel, U., Hasinger, G., & Pfeffermann, E. 1992, ApJ, 393, 819
- Stanford, S. A., Holden, B., Rosati, P., Tozzi, P., Borgani, S., Eisenhardt, P. R., & Spinrad, H. 2001, ApJ, in press, astro-ph/0012250
- Stocke, J. T., Liebert, J., Gioia, I. M., Maccacaro, T., Griffiths, R. E., Danziger, I. J., Kunth, D., & Lub, J. 1983, ApJ, 273, 458

- Stocke, J. T., Morris, S. L., Gioia, I. M., Maccacaro, T., Schild, R., Wolter, A., Fleming, T. A., & Henry, J. P. 1991, *ApJS*, 76, 813
- Stocke, J. T., Perlman, E. S., Gioia, I. M., & Harvanek, M. 1999, *AJ*, 117, 1967
- Struble, M. F., & Rood, H. J. 1991, *ApJ*, 374, 395
- Sutherland, W. 1988, *MNRAS*, 234, 159
- van Haarlem, M. P., Frenk, C. S., & White, S. D. M., 1997, *MNRAS*, 287, 817
- Viana, P. T. P., & Liddle, A. R. 1996, *MNRAS*, 281, 323
- Vikhlinin, A., McNamara, B. R., Forman, W., Jones, C., Quintana, H., & Hornstrup, A. 1998, *ApJ*, 502, 558
- Vikhlinin, A., McNamara, B. R., Forman, W., Jones, C., Quintana, H., & Hornstrup, A. 1998, *ApJ*, 498, L21
- White, N. E., Giommi, P., & Angelini, L. 1995, <http://heasarc.gsfc.nasa.gov/wgacat/wgacat.html>
- White, R. L., Becker, R. H., Helfand, D. J., & Gregg, M. D. 1997, *ApJ*, 475, 479
- White, D. A., Jones, C., & Forman, W., 1997, *MNRAS*, 292, 419
- Xue, Y., & Wu, X. 2001, *ApJ*, in press, astro-ph/0101529

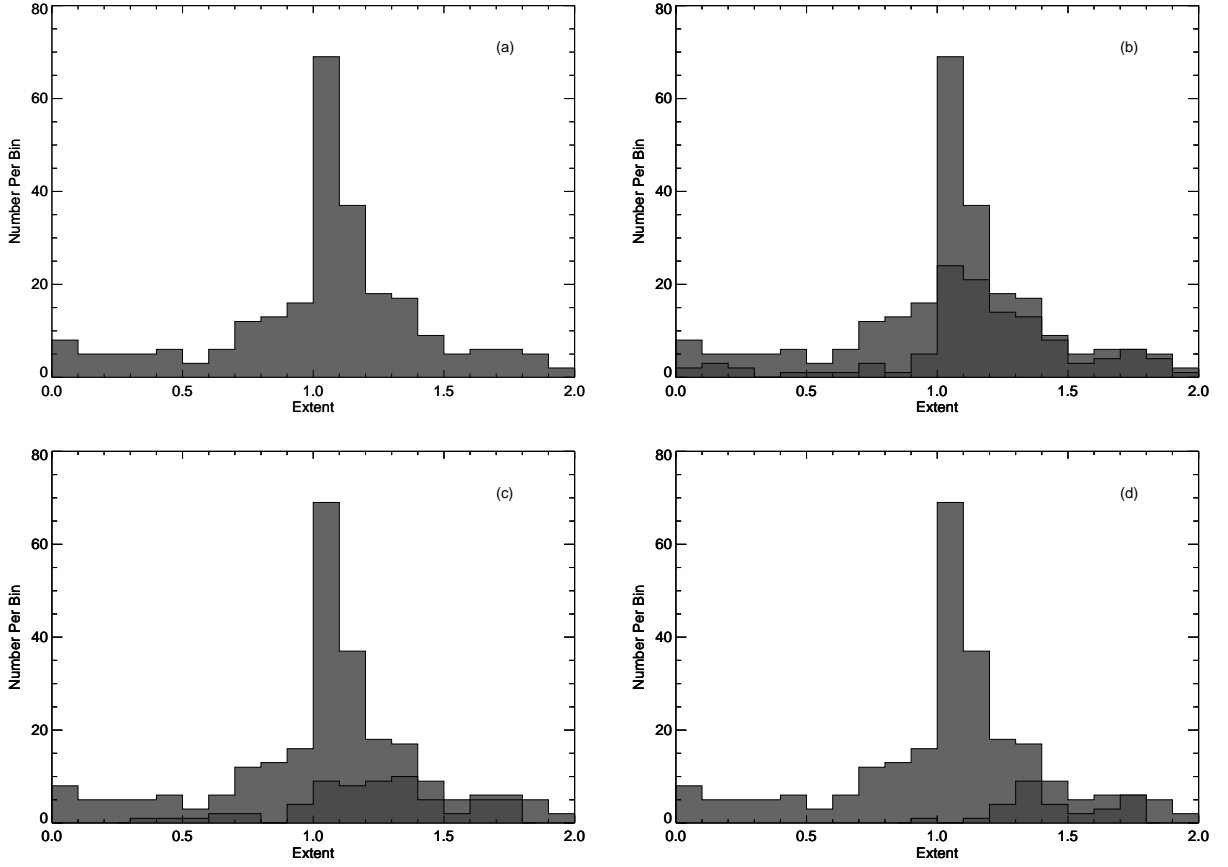


Fig. 1.— Histogram of the extent parameter for (a) all sources, (b) with sources selected for imaging, (c) with sources selected for spectroscopy, and (d) with confirmed clusters.



Fig. 2.— Overlays of the observed X-ray emission for the 60 extended or marginally extended sources on digitized plates from the POSS-I, UKST, or POSS-II surveys. Overlays for four additional X-ray sources which were found to be pointlike by VTP but were included as cluster candidates following our optical imaging program, are included at the end of the Figure. Each image is  $5' \times 5'$  with the standard orientation of north up and east to the left. The x-rays were smoothed with a  $45''$  Gaussian.

Fig. 3.— Overlays of the observed X-ray emission for each cluster on an optical (R-band) CCD image. Each image is 1.5 Mpc across at the cluster redshift (or  $5'$  if the redshift is unknown) with axes labelled in arc seconds from the VTP centroid with the standard orientation of north up and east to the left. The x-rays were smoothed with a  $45''$  Gaussian. Radio sources are labelled R1, R2, etc. as in Table 6 and are marked with a circle the size of the positional error given in the Table (which may be too small to see). Other sources (such as M stars) are also marked and labelled accordingly.

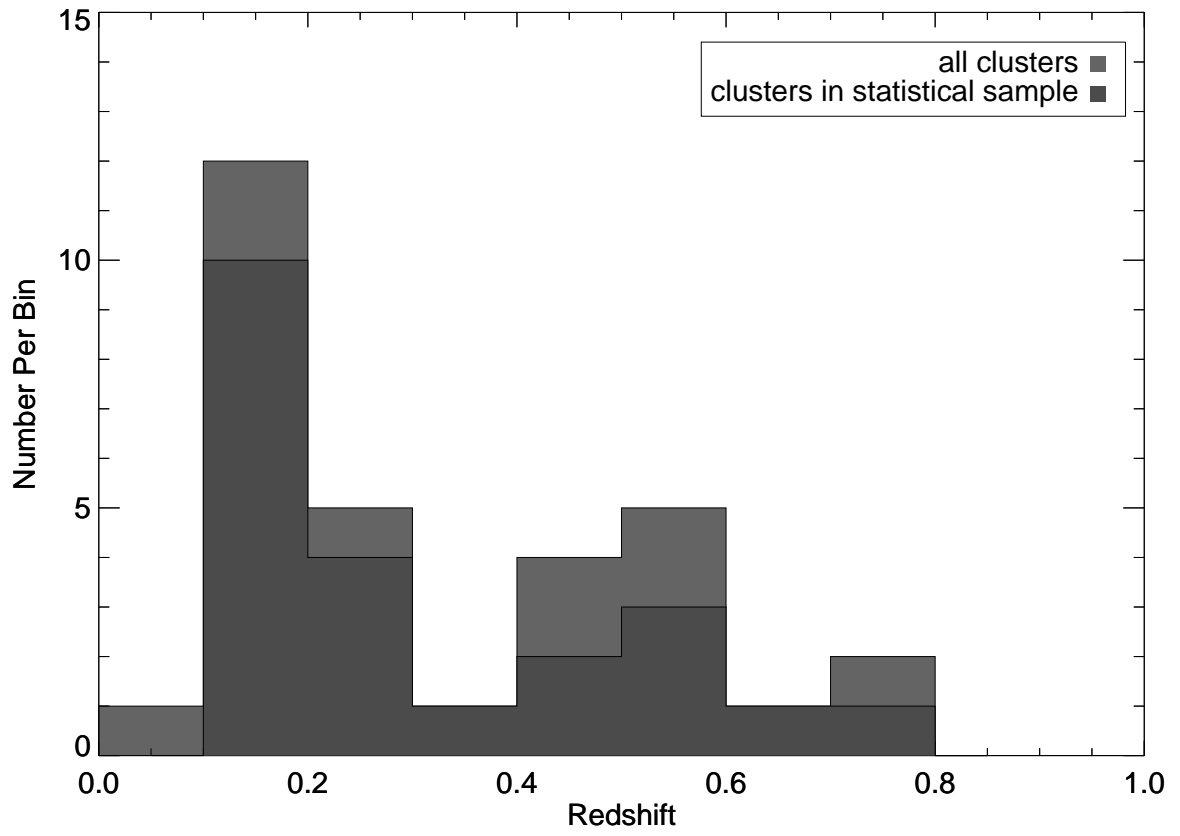


Fig. 4.— Redshift distribution of the cluster sample.

Table 1. ROSAT PSPC pointings used in WARPS

Sequence ID	Expo [sec.]	$\alpha$ (J2000)	$\delta$ (J2000)	Target Name
rp150071n00	17912	14 17 59.9	+5 08 23.9	NGC 5548
rp200125n00	8614	16 55 33.6	−08 23 24.1	LHS429
rp200474n00	9372	23 18 45.5	+2 36 00.1	KUV 2316+123
rp200905n00	10327	15 13 33.5	+8 34 11.8	SS BOOTIS
rp200965n00	10328	15 14 47.9	+4 01 47.8	PG1513+442
rp201007n00	18199	21 09 19.1	−13 14 24.1	LHS 65
rp201018n00	19015	15 18 11.9	+1 39 00.1	U CRB
rp201019n00	10639	11 13 11.9	−26 28 12.0	TT HYA
rp201037n00	15533	13 56 09.5	+5 55 12.0	ZZ BOO
rp201045n00	28336	00 39 19.2	+0 51 35.9	S AND
rp201070n00	8301	13 29 47.9	+1 06 00.0	HD117362
rp201471n00	8373	13 11 52.7	+7 52 48.1	HD 114710
rp201505n00	28004	18 42 38.3	+5 32 24.0	HD173524
rp300003n00	24464	02 06 52.7	+5 17 59.9	TT ARIETIS
rp300021n00	24506	16 05 45.6	+5 51 35.9	MS1603.6+2600
rp300028n00	27116	13 48 55.2	+7 57 35.8	PG1346+082
rp300043n00	14804	01 41 00.0	−67 53 24.1	BL HYI
rp300079n00	49502	03 37 55.2	−25 20 59.9	EXO 033319-2554.
rp300180n00	45541	17 17 07.2	+3 08 23.9	NGC 6341
rp300218n00	20662	20 38 14.4	−01 21 00.0	AE AQR
rp300220n00	15603	23 16 02.3	−05 27 00.0	RX J2316.1-0527
rp300389n00	36716	21 07 55.1	−05 16 12.1	RE2107-05
rp400116n00	8303	12 59 59.9	+2 40 11.9	PSR 1257+12
rp400293n00	20080	22 54 19.1	+9 03 36.1	GRB 910814
rp400322n00	12424	00 19 50.4	+1 56 59.9	RX J0019.8+2156
rp600119n00	11993	15 06 31.2	+5 46 12.0	NGC 5866
rp600164n00	16752	12 58 59.9	+4 51 36.0	NGC 4861
rp600439n00	11233	23 20 31.1	+7 13 48.0	III ZW 102
rp600448n00	12808	14 34 52.8	+8 40 48.0	MARK 474/NGC 568
rp600462n00	14242	14 15 33.5	+6 13 47.9	NGC 5529
rp700006n00	12146	21 14 52.8	+6 07 48.0	PG2112+059
rp700026n00	11197	04 22 14.3	−38 45 00.1	Q0420-388
rp700027a01	17554	02 09 28.7	−39 30 35.9	Q0207-398
rp700061n00	25728	14 06 57.6	+8 27 00.0	1404+286
rp700096n00	8038	15 59 09.6	+5 01 47.3	MKN493
rp700101n00	24337	00 08 19.1	+0 41 23.9	MKN335
rp700108n00	13683	01 43 57.6	+2 21 00.1	MKN573
rp700114n00	9451	02 28 38.4	−10 10 48.1	0226-1024
rp700117n00	22456	14 06 43.2	+4 11 23.6	3CR294
rp700122n00	27863	14 15 45.6	+1 29 42.0	Q1413+1143
rp700331n00	23437	00 48 45.6	+1 57 35.8	MKN 348
rp700350n00	10028	02 35 07.1	−04 01 48.0	0232-042
rp700377n00	10718	00 46 14.4	+1 04 11.8	Q0043+0048
rp700423n00	18562	23 03 14.4	+8 52 12.1	NGC 7469
rp700432n00	13860	02 07 50.3	+2 43 12.1	NAB 0205+024
rp700527n00	8898	14 19 04.7	−13 10 48.1	PG 1416-129
rp700794n00	10830	01 11 28.8	−38 04 48.0	NGC 424
rp700796n00	9004	13 10 57.5	+7 03 36.0	NGC 5005
rp700797n00	9516	13 25 43.2	−29 49 47.9	NGC 5135

Table 1—Continued

Sequence ID	Expo [sec.]	$\alpha$ (J2000)	$\delta$ (J2000)	Target Name
rp700908n00	9043	09 52 19.1	−01 36 35.9	MKN 1239
rp700920n00	12675	02 49 19.1	+9 17 59.8	MKN372
rp700976n00	11171	01 24 45.6	+9 18 35.8	MS0122.1+0903
rp700977n00	13951	02 08 38.3	+5 23 24.1	MS0205.7+3509
rp701000a01	27821	13 43 43.1	−00 14 59.8	BJS864
rp701018n00	11342	22 23 45.6	−02 13 12.1	3C445
rp701191n00	10395	22 12 59.9	−17 10 12.1	RX J2213.0-1710
rp701205n00	14428	23 43 31.2	−14 55 12.1	MS2340.9-1511
rp701206n00	9431	22 39 52.8	−05 52 11.9	BR 2237-06
rp701213n00	14664	15 52 09.5	+0 05 59.9	3C326
rp701250n00	18765	23 04 43.1	−08 41 23.4	MCG-2-58-22
rp701356n00	23554	02 37 12.0	−52 15 36.0	ESO198-G24/ WWHO
rp701373n00	15427	15 49 50.4	+1 25 48.1	3C 324
rp701403n00	11855	02 55 11.9	+0 10 48.0	NGC 1144
rp701405n00	13356	15 26 07.2	+1 40 11.8	NGC 5929
rp701411n00	22955	15 34 55.2	+3 29 24.1	ARP220
rp701420n00	9940	21 58 07.2	−15 01 11.9	2155-15
rp800003n00	28248	15 58 55.2	+3 23 23.8	GC1556+335
rp800150a01	12778	21 46 33.6	+4 13 47.9	21 HOUR FIELD
rp800401a01	11811	14 15 57.5	+3 07 11.9	4C23.37
rp800471n00	10639	04 30 45.6	+0 24 36.1	NGC 1588
rp800483n00	26671	00 22 52.7	+4 24 35.5	CL0020
rp900017n00	25815	04 40 55.1	−16 30 36.1	EDS - PSPC
rp900242n00	11620	04 14 16.8	−12 44 24.0	NGC 1535
rp900246n00	9152	04 11 40.7	−17 28 48.1	ERID1
rp900325n00	10322	13 17 43.1	+4 54 00.0	G107+71
rp900337n00	15618	22 25 48.0	−04 57 00.0	2223-052
rp900339n00	22143	22 53 57.5	+6 08 59.9	2251+158
rp900345n00	9346	21 27 55.2	+2 58 12.0	G064-26
rp900352n00	10383	02 17 19.1	−17 45 35.9	G192-67
rp900492n00	9609	03 48 23.9	−12 10 11.9	ERID4

Table 2. WARPS-I Source Catalog

Name	ROSAT Field	$\alpha$ (J2000)	$\delta$ (J2000)	$cr_{raw}$ [ $10^{-3}$ ]	$cr_{corr}$ [ $10^{-3}$ ]	$n_H$ [ $10^{20}$ ]	Flux [ $10^{-13}$ ]	Extent	Im	Sp	Id	Redshift/ Sp. Type	Other Name/ Notes
(1)	(2)	(3)	(4)	(5)	(6)	(7)	(8)	(9)	(10)	(11)	(12)	(13)	(14)
WARPJ0008.4+2034	rp700101n00	00 08 26.7	+20 34 31	13.894	15.934	3.95	2.10	1.07	...	...	qso	0.389	CRSS J0008.4+2034
WARPJ0008.8+2050	rp700101n00	00 08 53.9	+20 50 28	52.151	55.862	3.93	8.87	0.82	...	...	star	M(e)	CRSS J0008.9+2050
WARPJ0019.8+2202	rp400322n00	00 19 49.4	+22 02 51	4.027	4.894	4.14	0.65	1.13	R	Y	BLEND	...	M star+galaxy IC 1541
WARPJ0020.7+2205	rp400322n00	00 20 43.3	+22 05 36	6.143	11.651	4.14	1.54	1.81	R	Y	...	...	
WARPJ0038.2+3053	rp201045n00	00 38 12.4	+30 53 28	8.695	9.703	5.60	1.33	0.41	...	Y	gal	0.018	UGC 00381
WARPJ0040.2+3054	rp201045n00	00 40 12.1	+30 54 31	10.434	11.536	5.60	1.58	0.98	...	Y	BLEND	...	Sy1/QSO+NELG+Galaxy
WARPJ0045.2+0107	rp700377n00	00 45 16.8	+01 07 03	6.061	7.514	2.62	0.96	0.84	...	...	...	...	
WARPJ0111.0-3814	rp700794n00	01 11 05.4	-38 14 04	5.302	6.787	1.78	0.85	1.18	BR	Y	...	...	
WARPJ0111.6-3811	rp700794n00	01 11 36.0	-38 11 08	4.251	7.400	1.78	0.83	1.63	BR	Y	CLG	0.121	VMF 009
WARPJ0124.4+0921	rp700976n00	01 24 25.2	+09 21 40	5.358	6.166	4.70	0.98	1.05	...	...	star	...	GS 00614-00801
WARPJ0124.7+0929	rp700976n00	01 24 46.6	+09 29 35	3.119	6.739	4.79	0.91	1.92	R	...	...	...	possible blend,outskirts of NGC
WARPJ0124.8+0932	rp700976n00	01 24 48.6	+09 32 22	20.063	29.602	4.79	3.98	1.39	...	...	gal	.0081	NGC 524,SHARC
WARPJ0139.7-6749	rp300043n00	01 39 43.8	-67 49 12	18.353	20.043	2.35	2.55	0.33	...	...	...	...	5
WARPJ0140.5-6805	rp300043n00	01 40 31.3	-68 05 09	12.986	15.570	2.70	1.99	0.26	...	...	...	...	
WARPJ0141.1-6756	rp300043n00	01 41 10.2	-67 56 38	4.633	5.431	2.35	0.69	1.06	...	...	...	...	
WARPJ0141.8-6759	rp300043n00	01 41 51.0	-67 59 08	7.181	8.542	2.61	1.09	0.81	...	...	...	...	
WARPJ0143.8+0224	rp700108n00	01 43 48.7	+02 24 55	4.838	5.720	2.91	0.74	1.08	R	...	...	...	
WARPJ0144.5+0212	rp700108n00	01 44 30.3	+02 12 24	7.668	14.186	2.91	1.76	1.75	R	Y	CLG	0.165	VMF 019
WARPJ0144.5+0222	rp700108n00	01 44 31.9	+02 22 17	4.680	5.796	2.91	0.75	1.12	...	Y	AGN	1.024	
WARPJ0206.1+1512	rp300003n00	02 06 08.6	+15 12 32	7.102	7.889	6.18	1.10	1.02	R	Y	gal	0.043	IC 1777,RIXOS
WARPJ0206.3+1511	rp300003n00	02 06 23.7	+15 11 03	4.261	6.260	6.18	0.86	1.39	R	Y	CLG	0.251	VMF 022,RIXOS
WARPJ0206.4+1529	rp300003n00	02 06 24.6	+15 29 04	3.750	4.956	6.18	0.69	0.74	...	Y	NELG	0.301	RIXOS
WARPJ0207.3+0231	rp700432n00	02 07 22.5	+02 31 31	13.613	15.194	3.11	1.97	0.83	...	...	agn	0.673	MS 0204.8+0217
WARPJ0207.3+1509	rp300003n00	02 07 21.9	+15 09 38	4.056	4.752	6.18	0.66	0.55	R	Y	AGN	0.149	RIXOS F246 040,RIXOS
WARPJ0207.9+3518	rp700977n00	02 07 57.9	+35 18 34	5.457	6.063	6.26	0.84	1.37	...	Y	AGN	0.188	
WARPJ0210.4-3929	rp700027a01	02 10 26.7	-39 29 27	4.004	7.434	1.43	0.90	1.76	R	Y	CLG	0.273:	VMF 025
WARPJ0216.5-1747	rp900352n00	02 16 32.8	-17 47 11	7.962	13.422	2.98	1.75	1.60	R	Y	CLG	0.578	
WARPJ0217.4-1800	rp900352n00	02 17 26.5	-18 00 10	13.010	14.973	2.98	1.93	1.09	R	...	blend	...	SHARC,agn+?
WARPJ0217.7-1750	rp900352n00	02 17 46.5	-17 50 25	10.572	11.342	2.56	1.45	1.03	...	...	...	...	
WARPJ0227.7-1014	rp700114n00	02 27 42.8	-10 14 17	4.894	7.793	2.51	0.99	1.49	R	...	...	...	
WARPJ0228.1-1005	rp700114n00	02 28 11.7	-10 05 30	14.114	25.960	2.51	3.23	1.75	R	Y	CLG	0.149	VMF 026
WARPJ0229.2-1009	rp700114n00	02 29 13.7	-10 09 37	18.266	19.687	2.69	2.52	0.45	...	...	...	...	
WARPJ0229.5-1005	rp700114n00	02 29 35.4	-10 05 55	11.006	12.622	2.69	1.62	1.06	...	Y	...	...	
WARPJ0235.3-0347	rp700350n00	02 35 19.4	-03 47 11	27.030	28.997	2.70	3.71	0.67	...	...	agn	0.376	MS 0232.8-0400
WARPJ0235.5-0351	rp700350n00	02 35 34.9	-03 51 48	6.578	7.243	2.70	0.93	1.04	...	...	...	...	

Table 2—Continued

Name	ROSAT Field	$\alpha$ (J2000)	$\delta$ (J2000)	$cr_{raw}$ [ $10^{-3}$ ]	$cr_{corr}$ [ $10^{-3}$ ]	$n_H$ [ $10^{20}$ ]	Flux [ $10^{-13}$ ]	Extent	Im	Sp	Id	Redshift/ Sp. Type	Other Name/ Notes
(1)	(2)	(3)	(4)	(5)	(6)	(7)	(8)	(9)	(10)	(11)	(12)	(13)	(14)
WARPJ0236.1–5219	rp701356n00	02 36 11.8	−52 19 13	5.783	6.383	3.08	0.83	1.09	R	...	...	...	
WARPJ0236.5–5227	rp701356n00	02 36 30.1	−52 27 01	5.372	6.482	3.08	0.84	0.64	...	...	...	...	
WARPJ0236.8–5203	rp701356n00	02 36 51.6	−52 03 00	137.130	145.207	3.07	23.04	1.06	...	...	star	M2	EXO 0235.2-5216
WARPJ0237.0–5223	rp701356n00	02 37 01.9	−52 23 47	56.271	59.694	3.07	7.71	0.12	...	...	agn	0.113	EXO 0235.3-5236
WARPJ0237.2–5227	rp701356n00	02 37 13.6	−52 27 32	16.112	17.393	3.07	2.25	0.51	...	...	...	...	
WARPJ0238.0–5224	rp701356n00	02 38 01.2	−52 24 41	30.397	40.674	3.07	5.18	1.28	R	Y	CLG	0.135	A3038,VMF 028,SHARC
WARPJ0250.0+1908	rp700920n00	02 50 03.5	+19 08 00	6.852	11.547	9.87	1.68	1.56	BR	Y	CLG	0.122	SHARC
WARPJ0255.0+0017	rp701403n00	02 55 01.3	+00 17 49	21.072	22.680	6.48	3.17	1.04	R	...	...	...	
WARPJ0255.0+0025	rp701403n00	02 55 05.7	+00 25 26	33.471	35.758	6.64	5.02	0.99	...	Y	qso	0.354	US 3333
WARPJ0256.0+0015	rp701403n00	02 56 04.0	+00 15 55	5.431	7.821	6.64	1.10	1.35	R	Y	BLEND	...	NELG (z=0.14) + ?
WARPJ0337.4–2518	rp300079n00	03 37 28.6	−25 18 48	4.799	6.046	1.55	0.75	1.16	R	...	...	...	
WARPJ0337.5–2518	rp300079n00	03 37 35.2	−25 18 10	12.108	14.021	1.55	1.75	1.08	R	...	...	...	SHARC
WARPJ0337.6–2523	rp300079n00	03 37 37.9	−25 23 23	5.759	6.545	1.55	0.82	1.05	R	...	...	...	
WARPJ0338.4–2524	rp300079n00	03 38 27.6	−25 23 59	5.152	5.746	1.55	0.72	0.86	...	...	...	...	38
WARPJ0338.6–2529	rp300079n00	03 38 36.0	−25 29 10	8.171	9.553	1.55	1.19	0.87	...	...	...	...	—
WARPJ0347.6–1217	rp900492n00	03 47 40.7	−12 16 59	3.651	5.040	3.84	0.66	1.22	R	...	...	...	
WARPJ0347.8–1217	rp900492n00	03 47 50.4	−12 17 01	3.948	5.057	3.84	0.67	1.08	R	Y	...	...	
WARPJ0348.1–1201	rp900492n00	03 48 08.7	−12 01 34	5.051	7.398	3.80	0.97	1.38	R	Y	CLG	0.488	
WARPJ0349.3–1205	rp900492n00	03 49 18.7	−12 05 43	6.414	7.852	3.80	1.03	0.94	...	...	...	...	
WARPJ0411.5–1717	rp900246n00	04 11 34.7	−17 17 25	5.909	6.875	2.52	0.88	1.05	...	Y	AGN	...	
WARPJ0411.9–1728	rp900246n00	04 11 58.4	−17 28 04	8.347	9.800	2.49	1.25	1.10	...	...	...	...	
WARPJ0421.7–3847	rp700026n00	04 21 47.1	−38 47 47	4.409	6.044	1.90	0.76	1.26	R	...	...	...	
WARPJ0421.8–3833	rp700026n00	04 21 52.5	−38 33 00	3.777	5.587	1.90	0.70	0.53	...	...	...	...	
WARPJ0422.3–3832	rp700026n00	04 22 20.8	−38 32 20	4.843	6.719	1.90	0.84	6.79	...	...	qso	0.482	MS 0420.6-3839
WARPJ0440.8–1635	rp900017n00	04 40 53.2	−16 35 22	9.930	10.747	4.69	1.71	0.15	R	...	star	G0	1E 0438.6-1641
WARPJ0441.0–1616	rp900017n00	04 41 05.2	−16 16 08	9.427	10.916	4.69	1.47	1.03	R	...	...	...	
WARPJ0951.7–0128	rp700908n00	09 51 47.0	−01 28 30	2.995	5.536	3.84	0.73	1.73	R	Y	CLG	0.568	VMF 076
WARPJ0952.1–0148	rp700908n00	09 52 08.5	−01 48 20	3.777	6.230	3.84	0.82	1.56	R	...	...	...	VMF 077
WARPJ0952.5–0137	rp700908n00	09 52 34.8	−01 37 53	4.047	5.307	3.84	0.70	1.22	...	...	...	...	
WARPJ0952.7–0130	rp700908n00	09 52 43.3	−01 30 47	9.761	11.503	3.84	1.51	1.10	...	Y	BLEND	...	QSO (z=1.26)+K star
WARPJ1112.8–2619	rp201019n00	11 12 50.5	−26 19 07	8.632	10.461	5.47	1.43	1.12	IR	...	...	...	
WARPJ1113.0–2615	rp201019n00	11 13 05.7	−26 15 36	4.096	5.424	5.47	0.75	1.21	IR	Y	CLG	0.725	
WARPJ1259.1+3501	rp600164n00	12 59 09.2	+35 01 15	5.418	6.292	1.22	0.78	0.83	...	...	...	...	
WARPJ1259.5+1226	rp400116n00	12 59 33.3	+12 26 47	4.049	8.065	2.27	1.02	1.82	R	...	...	...	
WARPJ1300.0+3450	rp600164n00	13 00 03.0	+34 50 40	3.658	5.330	1.20	0.66	1.04	...	...	...	...	FIRST

Table 2—Continued

Name	ROSAT Field	$\alpha$ (J2000)	$\delta$ (J2000)	$cr_{raw}$ [ $10^{-3}$ ]	$cr_{corr}$ [ $10^{-3}$ ]	$n_H$ [ $10^{20}$ ]	Flux [ $10^{-13}$ ]	Extent	Im	Sp	Id	Redshift/ Sp. Type	Other Name/ Notes
(1)	(2)	(3)	(4)	(5)	(6)	(7)	(8)	(9)	(10)	(11)	(12)	(13)	(14)
WARPJ1316.4+4454	rp900325n00	13 16 25.7	+44 54 18	21.064	23.867	1.45	2.97	0.93	...	...	...	...	
WARPJ1317.4+4456	rp900325n00	13 17 28.3	+44 56 40	5.406	6.970	1.54	0.87	1.19	...	...	...	...	
WARPJ1318.6+4500	rp900325n00	13 18 39.9	+45 00 48	4.705	6.040	1.78	0.76	1.19	R	Y	BLEND	0.173	AGN (z=0.173:) + ?
WARPJ1328.9+0112	rp201070n00	13 28 56.1	+01 12 15	4.356	6.759	1.85	0.85	3.15	R	...	...	...	
WARPJ1343.0-0013	rp701000a01	13 43 02.6	-00 13 01	7.140	8.625	1.91	1.08	3.00	...	...	...	...	
WARPJ1348.5+0757	rp300028n00	13 48 34.9	+07 57 37	7.305	8.087	2.00	1.28	0.08	...	...	star	F5	HD 120317
WARPJ1356.1+2606	rp201037n00	13 56 09.6	+26 06 41	4.794	6.227	1.30	0.77	1.20	R	Y	BLEND	1.320	QSO (z=1.32) + ?
WARPJ1356.3+2552	rp201037n00	13 56 22.0	+25 52 49	4.670	5.442	1.34	0.67	1.06	R	...	...	...	
WARPJ1406.2+2830	rp700061n00	14 06 16.1	+28 30 55	4.739	7.065	1.46	0.87	1.39	R	Y	CLG	0.546	VMF 153
WARPJ1406.9+2834	rp700061n00	14 06 55.4	+28 34 25	11.321	19.056	1.46	2.25	1.58	BR	Y	CLG	0.117	VMF 154,SHARC
WARPJ1407.3+2818	rp700061n00	14 07 19.5	+28 18 19	14.814	16.501	1.46	2.05	0.48	...	...	qso	1.121	CRSS J1407.3+2818
WARPJ1407.7+2830	rp700061n00	14 07 45.5	+28 30 31	26.856	30.942	1.46	3.85	0.81	R	...	qso	0.642	CRSS J1407.7+2830,FIRST
WARPJ1415.1+3612	rp600462n00	14 15 11.1	+36 12 03	6.295	9.132	1.14	1.13	1.36	R	...	CLG	[0.7]	FIRST
WARPJ1415.2+1119	rp700122n00	14 15 16.8	+11 19 30	2.855	4.671	1.80	0.74	1.40	R	...	star	G	CRSS J1415.2+1119
WARPJ1415.2+3608	rp600462n00	14 15 12.4	+36 08 09	14.248	15.377	1.14	1.90	0.99	...	...	...	...	
WARPJ1415.5+1131	rp700122n00	14 15 31.8	+11 31 57	10.341	11.810	1.80	1.48	1.06	...	...	qso	0.256	CRSS J1415.5+1131
WARPJ1415.6+1124	rp700122n00	14 15 40.3	+11 24 10	3.865	4.388	1.80	0.70	0.77	...	...	star	M(e)	CRSS J1415.6+1124
WARPJ1417.3+2505	rp150071n00	14 17 22.1	+25 05 22	13.475	14.796	1.58	1.84	0.44	...	...	...	...	
WARPJ1417.3+2513	rp150071n00	14 17 23.2	+25 13 41	5.259	6.691	1.58	0.83	0.21	...	...	qso	0.56	2E 1416.6+2523
WARPJ1418.5+2511	rp150071n00	14 18 31.8	+25 10 59	39.210	48.915	1.93	6.20	1.18	R	Y	CLG	0.296	VMF 159,SHARC
WARPJ1418.6-1306	rp700527n00	14 18 38.1	-13 06 36	5.468	6.230	6.29	0.87	1.02	...	...	...	...	
WARPJ1418.9+2509	rp150071n00	14 18 58.2	+25 09 49	7.580	8.535	1.93	1.07	0.73	...	...	qso	0.674	[HB89] 1416+254
WARPJ1419.5-1321	rp700527n00	14 19 33.2	-13 21 13	4.541	6.819	7.11	0.97	1.38	R	...	...	...	
WARPJ1419.6-1316	rp700527n00	14 19 39.3	-13 16 35	6.108	7.011	7.11	1.00	1.05	R	...	...	...	
WARPJ1435.4+4845	rp600448n00	14 35 29.0	+48 45 17	4.407	6.475	2.05	0.82	1.38	...	...	gal	0.0072	NGC 5689
WARPJ1505.4+5540	rp600119n00	15 05 24.1	+55 40 34	4.584	5.282	1.47	0.84	0.81	...	...	star	F8	HD 134023
WARPJ1505.7+5549	rp600119n00	15 05 43.9	+55 49 33	8.573	10.047	1.47	1.25	1.08	...	...	...	...	
WARPJ1506.8+5532	rp600119n00	15 06 51.1	+55 32 06	5.806	7.474	1.47	0.93	0.84	...	...	...	...	
WARPJ1513.5+3846	rp200905n00	15 13 32.3	+38 46 00	6.307	7.328	1.39	0.91	0.41	R	...	...	...	
WARPJ1513.8+4400	rp200965n00	15 13 48.9	+44 00 06	5.331	6.599	1.95	0.83	1.16	R	...	...	...	
WARPJ1515.6+4411	rp200965n00	15 15 39.1	+44 11 29	9.071	10.275	2.04	1.29	1.04	R	...	...	...	
WARPJ1517.0+3140	rp201018n00	15 17 03.6	+31 40 45	5.334	6.127	1.91	0.77	0.97	R	...	...	...	SHARC
WARPJ1517.2+3141	rp201018n00	15 17 13.0	+31 41 25	5.260	6.160	1.91	0.98	0.67	R	...	star	G5	PPM 78477,FIRST
WARPJ1519.3+3139	rp201018n00	15 19 19.6	+31 39 07	5.401	6.068	1.90	0.76	0.04	R	...	...	...	
WARPJ1524.9+4143	rp701405n00	15 24 59.9	+41 43 37	9.035	10.256	2.08	1.29	1.05	...	...	...	...	FIRST

Table 2—Continued

Name	ROSAT Field	$\alpha$ (J2000)	$\delta$ (J2000)	$cr_{raw}$ [ $10^{-3}$ ]	$cr_{corr}$ [ $10^{-3}$ ]	$n_H$ [ $10^{20}$ ]	Flux [ $10^{-13}$ ]	Extent	Im	Sp	Id	Redshift/ Sp. Type	Other Name/ Notes
(1)	(2)	(3)	(4)	(5)	(6)	(7)	(8)	(9)	(10)	(11)	(12)	(13)	(14)
WARPJ1525.1+4145	rp701405n00	15 25 10.2	+41 45 58	4.360	5.195	2.08	0.66	1.10	...	...	...	...	
WARPJ1525.8+4139	rp701405n00	15 25 49.1	+41 39 28	4.134	5.820	2.08	0.73	1.31	...	...	BLEND	...	
WARPJ1525.9+4148	rp701405n00	15 25 58.2	+41 48 36	7.995	9.170	2.08	1.16	1.07	...	...	...	...	
WARPJ1527.1+4133	rp701405n00	15 27 08.8	+41 33 12	5.721	7.750	2.08	1.23	0.31	...	...	star	G5	HD 137896,FIRST
WARPJ1548.8+2120	rp701373n00	15 48 51.9	+21 20 27	7.421	8.665	4.30	1.15	1.05	...	...	...	...	
WARPJ1549.7+2114	rp701373n00	15 49 43.2	+21 14 02	16.453	18.612	4.30	2.48	1.12	...	...	...	...	
WARPJ1550.2+2124	rp701373n00	15 50 15.1	+21 24 30	4.658	5.046	4.30	0.67	1.03	...	...	...	...	
WARPJ1552.0+2013	rp701213n00	15 52 02.5	+20 13 58	70.435	80.424	3.70	10.55	1.07	R	...	qso	0.250	[HB89] 1549+203
WARPJ1552.2+2013	rp701213n00	15 52 12.5	+20 13 32	11.883	25.704	3.70	3.29	2.04	BR	Y	CLG	0.135	VMF 175,SHARC
WARPJ1552.4+2007	rp701213n00	15 52 29.8	+20 07 18	24.633	28.092	3.70	3.69	1.06	R	...	...	...	RadioS
WARPJ1558.1+3500	rp700096n00	15 58 09.7	+35 00 52	5.429	6.994	2.03	0.88	1.94	R	...	...	...	
WARPJ1558.7+3511	rp700096n00	15 58 43.6	+35 11 19	4.126	6.575	1.86	0.83	1.45	R	...	...	...	
WARPJ1655.4−0820	rp200125n00	16 55 29.3	−08 20 00	1268.800	1344.763	13.38	213.40	1.28	...	...	star	M3Ve	V1054 Oph
WARPJ1656.1−0819	rp200125n00	16 56 11.7	−08 19 10	4.996	5.983	13.38	0.97	0.01	...	...	...	...	
WARPJ1716.5+4302	rp300180n00	17 16 32.6	+43 02 27	53.605	57.084	2.19	9.06	0.67	...	Y	STAR	G/K	in NGC 6341
WARPJ1841.5+5531	rp201505n00	18 41 31.1	+55 31 17	4.598	5.269	4.95	0.71	1.68	...	Y	AGN	...	
WARPJ1841.8+5540	rp201505n00	18 41 50.9	+55 40 48	6.510	7.783	4.95	1.05	1.08	...	Y	...	...	RadioS
WARPJ1842.7+5529	rp201505n00	18 42 43.9	+55 29 22	31.186	33.249	4.95	4.49	1.09	...	Y	...	...	RadioS
WARPJ1843.4+5527	rp201505n00	18 43 26.7	+55 27 44	4.357	5.708	4.95	0.77	1.23	...	Y	BLEND	...	
WARPJ2037.6−0125	rp300218n00	20 37 36.7	−01 25 28	17.696	19.070	7.02	2.70	1.02	...	Y	AGN	0.132	
WARPJ2038.3−0106	rp300218n00	20 38 20.2	−01 06 19	9.960	11.400	7.02	1.81	4.85	...	...	star	G8/K0	HD 196574
WARPJ2038.4−0125	rp300218n00	20 38 29.6	−01 25 11	2.654	4.842	7.02	0.70	1.71	BR	Y	CLG	0.679	
WARPJ2038.7−0114	rp300218n00	20 38 47.9	−01 14 24	15.851	17.455	7.02	2.47	1.06	...	...	...	...	
WARPJ2107.6−0512	rp300389n00	21 07 36.6	−05 12 11	11.022	12.464	5.57	1.71	1.05	...	...	...	...	
WARPJ2108.6−1316	rp201007n00	21 08 40.7	−13 16 46	7.547	8.599	4.09	1.14	1.03	...	...	...	...	
WARPJ2108.8−0516	rp300389n00	21 08 51.0	−05 16 32	9.330	13.706	5.57	1.89	1.40	R	Y	CLG	0.317	VMF 200
WARPJ2109.3−1310	rp201007n00	21 09 21.1	−13 10 58	3.308	4.096	4.09	0.65	1.13	...	...	star	F8	HD 358246
WARPJ2115.2+0608	rp700006n00	21 15 16.4	+06 08 43	10.952	12.826	6.62	1.80	1.09	...	Y	qso	0.398	[HB89] 2112+059
WARPJ2126.9+1257	rp900345n00	21 26 54.5	+12 57 39	8.179	10.032	6.38	1.40	1.10	...	Y	AGN	0.82	
WARPJ2127.0+1251	rp900345n00	21 27 02.4	+12 51 10	5.202	6.743	6.38	0.94	0.61	...	Y	AGN	0.22	
WARPJ2158.4−1450	rp701420n00	21 58 28.7	−14 50 34	4.140	7.238	3.75	0.95	1.63	R	Y	BLEND	1.075	QSO (z=1.08) + ?
WARPJ2158.9−1452	rp701420n00	21 58 55.2	−14 52 53	3.951	5.128	3.75	0.67	1.11	R	...	...	...	
WARPJ2223.5−0218	rp701018n00	22 23 32.8	−02 18 04	9.678	11.105	4.95	1.76	1.07	...	...	star	F8	HD 212337
WARPJ2223.8−0206	rp701018n00	22 23 48.6	−02 06 19	19.832	26.063	4.95	3.52	1.24	R	...	agn	0.056	3C 445,SHARC,FIRST
WARPJ2224.3−0218	rp701018n00	22 24 22.7	−02 18 33	5.917	7.770	4.95	1.05	1.23	R	...	...	...	



Table 2—Continued

Name	ROSAT	$\alpha$	$\delta$	$cr_{raw}$	$cr_{corr}$	$n_H$	Flux	Extent	Im	Sp	Id	Redshift/ Sp. Type	Other Name/ Notes
(1)	(2)	(3)	(4)	(5)	(6)	(7)	(8)	(9)	(10)	(11)	(12)	(13)	(14)
WARPJ2225.0−0457	rp900337n00	22 25 00.5	−04 57 51	5.670	6.554	5.07	0.89	0.77	R	...	...	...	
WARPJ2239.4−0547	rp701206n00	22 39 24.8	−05 47 10	15.813	21.800	4.01	2.88	1.30	BR	Y	CLG	0.242	A2465S,VMF 208
WARPJ2239.6−0543	rp701206n00	22 39 39.6	−05 43 15	17.600	30.484	4.01	4.04	1.65	BR	Y	CLG	0.243	A2465N,VMF 210
WARPJ2253.5+2852	rp400293n00	22 53 35.2	+28 52 11	5.336	6.187	5.60	0.85	0.77	R	...	...	...	
WARPJ2253.6+2913	rp400293n00	22 53 37.6	+29 13 13	21.089	22.997	5.68	3.16	0.74	...	...	...	...	
WARPJ2254.1+1606	rp900339n00	22 54 10.9	+16 06 56	9.188	9.921	6.54	1.39	1.04	...	...	...	...	
WARPJ2254.8+1604	rp900339n00	22 54 49.8	+16 04 21	10.281	11.276	6.54	1.58	0.99	...	Y	...	...	
WARPJ2255.4+2905	rp400293n00	22 55 26.1	+29 05 28	4.258	5.416	5.68	0.74	1.12	R	...	...	...	
WARPJ2302.7+0845	rp700423n00	23 02 46.4	+08 45 20	3.803	5.225	5.28	0.71	0.19	R	...	...	...	
WARPJ2302.8+0843	rp700423n00	23 02 48.1	+08 43 50	4.628	5.239	4.86	0.72	0.92	R	Y	CLG	0.722	
WARPJ2302.9+0839	rp700423n00	23 02 54.7	+08 39 04	4.470	5.571	4.86	0.75	0.22	R	...	...	...	
WARPJ2303.0+0846	rp700423n00	23 03 01.0	+08 46 55	5.453	6.037	4.86	0.81	0.71	...	...	...	...	
WARPJ2304.0−0837	rp701250n00	23 04 00.5	−08 37 52	5.346	6.553	3.51	0.86	0.01	...	...	...	...	
WARPJ2319.5+1226	rp200474n00	23 19 34.6	+12 26 21	21.225	31.721	4.42	4.15	1.42	R	Y	CLG	0.124	VMF 217,FRIXOS
WARPJ2320.7+1659	rp600439n00	23 20 46.1	+16 59 45	3.430	5.279	4.38	0.70	1.44	R	Y	BLEND	0.499	AGN (z=1.8)+CLG (z=0.50)
WARPJ2320.9+1715	rp600439n00	23 20 57.8	+17 15 10	14.326	15.559	4.68	2.47	0.79	...	...	star	A9/F0	HD 220091

Table 3. Other Sources

Name	ROSAT Field	$\alpha$ (J2000)	$\delta$ (J2000)	$cr_{raw}$ [ $10^{-3}$ ]	$cr_{corr}$ [ $10^{-3}$ ]	$n_H$ [ $10^{20}$ ]	Flux [ $10^{-13}$ ]	Extent	Im	Sp	Id	Redshift/ Sp. Type	Other Name/ Notes
(1)	(2)	(3)	(4)	(5)	(6)	(7)	(8)	(9)	(10)	(11)	(12)	(13)	(14)
WARPJ0019.5+2156	rp400322n00	00 19 34.7	+21 56 24	3.261	4.091	4.28	0.54	1.16	R	...	...	...	
WARPJ0038.5+3058	rp201045n00	00 38 34.2	+30 58 22	3.240	3.794	5.60	0.52	0.77	...	Y	QSO	1.326	
WARPJ0045.8+0107	rp700377n00	00 45 50.3	+01 07 24	3.447	4.353	2.62	0.56	0.94	R	...	...	...	
WARPJ0110.7−3813	rp700794n00	01 10 44.9	−38 13 28	3.538	4.477	1.78	0.56	1.16	R	...	...	...	
WARPJ0207.1+1504	rp300003n00	02 07 06.8	+15 04 54	3.233	4.303	6.18	0.60	0.72	R	...	...	...	RIXOS
WARPJ0216.9−1753	rp900352n00	02 16 57.9	−17 53 58	3.169	3.838	2.98	0.49	1.12	R	...	...	...	
WARPJ0234.2−0356	rp700350n00	02 34 13.3	−03 56 51	3.624	5.114	2.59	0.64	1.31	R	Y	CLG	0.447	
WARPJ0236.0−5224	rp701356n00	02 36 04.2	−52 24 50	3.472	4.064	3.08	0.53	1.09	R	...	...	...	VMF 027
WARPJ0236.7−5209	rp701356n00	02 36 47.9	−52 09 22	3.584	4.007	3.07	0.52	0.14	R	...	...	...	
WARPJ0255.3+0004	rp701403n00	02 55 23.1	+00 04 38	3.627	4.584	6.48	0.64	1.18	R	...	...	...	
WARPJ0255.4−0002	rp701403n00	02 55 27.9	−00 02 24	3.190	4.581	6.48	0.64	1.35	R	...	blend	...	AGN (Q 0252-0014)+?
WARPJ0347.8−1158	rp900492n00	03 47 50.3	−11 58 43	3.002	3.911	3.80	0.51	1.04	R	...	...	...	—
WARPJ0412.4−1724	rp900246n00	04 12 30.0	−17 24 38	3.818	4.916	2.52	0.63	1.18	R	...	...	...	42
WARPJ0414.4−1236	rp900242n00	04 14 25.2	−12 36 41	3.970	4.614	3.70	0.61	0.03	R	...	...	...	—
WARPJ0414.7−1240	rp900242n00	04 14 43.2	−12 40 04	3.008	3.714	3.70	0.49	1.08	R	...	...	...	
WARPJ0440.6−1636	rp900017n00	04 40 39.1	−16 36 05	3.147	4.228	4.69	0.57	1.24	R	...	...	...	
WARPJ1311.1+3711	rp700796n00	13 11 11.0	+37 11 57	3.460	3.988	1.11	0.49	1.16	R	...	...	...	
WARPJ1318.8+4457	rp900325n00	13 18 52.8	+44 57 42	3.734	4.262	1.54	0.53	1.03	R	...	...	...	
WARPJ1349.0+0750	rp300028n00	13 49 02.3	+07 50 44	3.169	3.852	2.05	0.49	1.06	R	...	...	...	
WARPJ1407.6+3415	rp700117n00	14 07 40.5	+34 15 18	3.404	4.729	1.20	0.58	1.30	R	Y	CLG	0.577	
WARPJ1407.7+2824	rp700061n00	14 07 45.6	+28 24 42	3.057	4.322	1.46	0.54	0.92	R	...	qso	1.127	CRSS J1407.7+2824
WARPJ1415.0+1119	rp700122n00	14 15 04.5	+11 19 35	2.671	3.649	1.80	0.46	1.02	R	...	qso	0.538	CRSS J1415.0+1119
WARPJ1415.6+3622	rp600462n00	14 15 39.0	+36 22 11	4.010	5.098	0.99	0.63	1.19	R	...	gal	0.0159	KUG 1413+366
WARPJ1501.0−0824	rp200510n00	15 01 04.3	−08 24 56	3.029	3.419	7.33	0.49	0.69	R	N	...	0.51	estimated redshift
WARPJ1515.6+4346	rp200965n00	15 15 31.9	+43 46 18	15.821	24.478	1.96	2.98	1.48	R	Y	CLG	0.135	VMF 169
WARPJ1517.9+3127	rp201018n00	15 17 55.9	+31 27 35	3.016	4.570	1.90	0.57	1.43	R	Y	CLG	0.744	...
WARPJ1535.1+2336	rp701411n00	15 35 06.0	+23 36 55	4.190	4.589	4.29	0.61	1.19	...	Y	AGN	1.25	
WARPJ1537.7+1201	rp400117n00	15 37 43.0	+12 01 14	5.512	10.520	3.44	1.29	...	R	Y	CLG	0.136	VMF 171
WARPJ1552.1+2017	rp701213n00	15 52 07.8	+20 17 39	3.196	3.722	3.70	0.49	1.00	R	...	...	...	
WARPJ1605.2+2541	rp300021n00	16 05 17.2	+25 41 23	3.306	4.405	4.62	0.59	0.21	R	...	qso	1.071	CRSS J1605.2+2541
WARPJ1605.6+2543	rp300021n00	16 05 39.7	+25 43 08	3.380	4.287	4.62	0.57	1.15	R	...	gal	0.278	CRSS J1605.6+2543
WARPJ1717.4+4319	rp300180n00	17 17 29.8	+43 19 41	3.662	4.446	2.19	0.56	0.40	...	Y	AGN	0.632	
WARPJ2108.6−0507	rp300389n00	21 08 39.9	−05 07 27	2.213	3.132	5.57	0.41	1.29	R	Y	CLG	0.222	
WARPJ2157.6−1506	rp701420n00	21 57 40.2	−15 06 58	3.674	4.650	3.75	0.61	1.16	R	...	...	...	
WARPJ2224.5−0208	rp701018n00	22 24 31.7	−02 08 05	3.011	3.671	4.95	0.50	0.91	BR	...	...	...	

Table 3—Continued

Name	ROSAT Field	$\alpha$ (J2000)	$\delta$ (J2000)	$cr_{raw}$ [ $10^{-3}$ ]	$cr_{corr}$ [ $10^{-3}$ ]	$n_H$ [ $10^{20}$ ]	Flux [ $10^{-13}$ ]	Extent	Im	Sp	Id	Redshift/ Sp. Type	Other Name/ Notes
(1)	(2)	(3)	(4)	(5)	(6)	(7)	(8)	(9)	(10)	(11)	(12)	(13)	(14)
WARPJ2224.6–0218	rp701018n00	22 24 41.2	−02 18 26	3.110	4.040	4.95	0.55	1.12	R	...	...	...	
WARPJ2239.5–0600	rp701206n00	22 39 35.4	−06 00 17	3.330	5.155	3.96	0.63	1.46	BR	Y	CLG	0.174	VMF 209
WARPJ2253.9+2911	rp400293n00	22 53 54.5	+29 11 46	3.126	3.603	5.68	0.50	1.86	...	Y	...	...	
WARPJ2315.2–0529	rp300220n00	23 15 14.6	−05 29 47	3.647	4.239	3.59	0.55	1.08	R	...	...	...	
WARPJ2316.4–0526	rp300220n00	23 16 25.1	−05 26 12	3.673	4.613	3.59	0.60	1.16	R	...	...	...	
WARPJ2318.0+1238	rp200474n00	23 18 06.0	+12 38 12	3.574	4.233	4.24	0.56	1.06	R	...	agn	0.713	RIXOS F294 001,RIXOS
WARPJ2343.4–1443	rp701205n00	23 43 27.6	−14 43 02	3.369	4.906	2.20	0.62	1.36	R	...	...	...	
WARPJ2343.4–1500	rp701205n00	23 43 26.3	−15 00 51	3.181	4.173	2.20	0.53	1.22	R	...	...	...	

Table 4. WARPS-I Statistically Complete, Flux Limited Sample

Name	$\alpha$ (J2000)	$\delta$ (J2000)	Extent	$n_H$ [ $10^{20}$ ]	Flux [ $10^{-13}$ ]	$\log L_x$	$r_c$ [ $''$ ]	z	$n_z$	Flags	Other Name/ Notes
(1)	(2)	(3)	(4)	(5)	(6)	(7)	(8)	(9)	(10)	(11)	(12)
WARPJ0111.6–3811	01 11 36.0	–38 11 08	1.63	1.78	0.83	42.75	18.4	0.121	3		VMF 009
WARPJ0144.5+0212	01 44 30.3	+02 12 24	1.75	2.91	1.76	43.34	42.5	0.165	2		VMF 019
WARPJ0206.3+1511	02 06 23.7	+15 11 03	1.39	6.18	0.86	43.40	19.2	0.251	2		VMF 022,RIXOS
WARPJ0210.4–3929	02 10 26.7	–39 29 27	1.76	1.43	0.90	43.49	39.4	0.273	2		VMF 025
WARPJ0216.5–1747	02 16 32.8	–17 47 11	1.60	2.98	1.75	44.41	39.1	0.578	3	c	
WARPJ0228.1–1005	02 28 11.7	–10 05 30	1.75	2.51	3.23	43.50	42.5	0.149	2	c	VMF 026
WARPJ0238.0–5224	02 38 01.2	–52 24 41	1.28	3.07	5.18	43.62	24.8	0.135	1		A3038, VMF 028, SHARC
WARPJ0250.0+1908	02 50 03.5	+19 08 00	1.56	9.87	1.68	43.05	21.2	0.122	2		SHARC
WARPJ0348.1–1201	03 48 08.7	–12 01 34	1.38	3.80	0.97	44.02	15.3	0.488	5		
WARPJ0951.7–0128	09 51 47.0	–01 28 30	1.73	3.84	0.73	44.03	24.2	0.568	1	c	VMF 076
WARPJ1113.0–2615	11 13 05.7	–26 15 36	1.21	5.47	0.75	44.26	6.7	0.725	2		
WARPJ1406.2+2830	14 06 16.1	+28 30 55	1.39	1.46	0.87	44.07	11.8	0.546	...		VMF 153
WARPJ1406.9+2834	14 06 55.4	+28 34 25	1.58	1.46	2.25	43.14	22.7	0.117	3	c	VMF 154, SHARC
WARPJ1415.1+3612	14 15 11.1	+36 12 03	1.36	1.14	1.13	44.39	11.6	[0.7]	...		FIRST
WARPJ1418.5+2511	14 18 31.8	+25 10 59	1.18	1.93	6.20	44.37	11.9	0.296	3		VMF 159, SHARC
WARPJ1552.2+2013	15 52 12.5	+20 13 32	2.04	3.70	3.29	43.43	35.7	0.135	3		VMF 175, SHARC
WARPJ2038.4–0125	20 38 29.6	–01 25 11	1.71	7.02	0.70	44.17	20.3	0.679	2		
WARPJ2108.8–0516	21 08 51.0	–05 16 32	1.40	5.57	1.89	43.93	29.7	0.317	10		VMF 200
WARPJ2239.4–0547	22 39 24.8	–05 47 10	1.30	4.01	2.88	43.87	16.3	0.242	6		A2465S, VMF 208
WARPJ2239.6–0543	22 39 39.6	–05 43 15	1.65	4.01	4.04	44.02	43.7	0.243	6		A2465N, VMF 210
WARPJ2302.8+0843	23 02 48.1	+08 43 50	0.92	4.86	0.72	44.23	0.1	0.722	1	c	
WARPJ2319.5+1226	23 19 34.6	+12 26 21	1.42	4.42	4.15	43.45	28.8	0.124	3		VMF 217,RIXOS

Table 5. WARPS-I Additional Clusters and Candidates

Name	$\alpha$ (J2000)	$\delta$ (J2000)	Extent	$n_H$ [ $10^{20}$ ]	Flux [ $10^{-13}$ ]	$\log L_x$	$r_c$ [ $''$ ]	z	$n_z$	Flags	Other Name/ Notes
(1)	(2)	(3)	(4)	(5)	(6)	(7)	(8)	(9)	(10)	(11)	(12)
WARPJ0022.0+0422	00 22 03.4	+04 22 38	1.81	2.87	0.72	43.74	28.8	0.407	5	8c	GHO 00190.5+0405
WARPJ0023.1+0421	00 23 06.0	+04 21 13	1.41	2.87	0.76	43.86	15.6	0.453	3	8	
WARPJ0210.2-3932	02 10 13.8	-39 32 50	1.77	1.43	0.46	42.89	19.8	[0.190]	...	<	VMF 024, estimated redshift
WARPJ0234.2-0356	02 34 13.3	-03 56 51	1.31	2.59	0.64	43.78	12.4	0.447	5	<	
WARPJ0236.0-5224	02 36 04.2	-52 24 50	1.09	3.08	0.53	...	4.2	...	-	?	VMF 027
WARPJ0255.3+0004	02 55 23.1	+00 04 38	1.18	6.48	0.64	...	5.3	...	-	?	
WARPJ1407.6+3415	14 07 40.5	+34 15 18	1.30	1.20	0.58	...	11.8	0.577	1	?	
WARPJ1415.3+2308	14 15 18.4	+23 08 57	1.50	1.79	0.57	42.02	15.4	0.064	5	8	
WARPJ1416.4+2315	14 16 26.9	+23 15 32	1.32	1.85	12.79	44.02	46.1	0.137	2	8c	SHARC
WARPJ1501.0-0824	15 37 43.0	+12 01 14	0.69	7.33	0.49	43.79	...	[0.51]	-	?	estimated redshift
WARPJ1515.5+4346	15 15 31.9	+43 46 18	...	1.96	...	...	...	0.135	3	b	VMF 169
WARPJ1517.9+3127	15 17 55.9	+31 27 35	1.43	1.90	0.57	44.16	0.41	0.744	2	<	
WARPJ1537.7+1201	15 37 43.0	+12 01 14	...	3.44	1.20	43.01	...	0.134	3	b	VMF 171
WARPJ2108.6-0507	21 08 39.9	-05 07 27	1.29	5.57	0.41	42.98	10.5	0.222	3	<	
WARPJ2146.0+0423	21 46 05.5	+04 23 13	1.33	5.42	1.84	44.36	20.0	0.532	4	8	VMF 204, GHO 2143+0408
WARPJ2239.5-0600	22 39 35.4	-06 00 17	1.46	3.96	0.63	42.95	20.2	0.174	2	<	VMF 209
WARPJ2320.7+1659	23 20 46.1	+16 59 45	1.44	4.38	0.70	...	18.5	0.499	3	<c	AGN (z=1.8)+CLG (z=0.50)

Table 6. Radio Sources within 2' of WARPS Cluster Candidates

Name	$\alpha$ (J2000)	$\delta$ (J2000)	Error [']	Dist [']	Flux [mJy]	Comments
WARPJ0144.5+0212:R1	01 44 29.89	+02 12 43.3	1	20	80.6	Just north of BCG
WARPJ0144.5+0212:R2	01 44 33.08	+02 11 41.6	4	59	8.9	
WARPJ0206.3+1511:R1	02 06 20.44	+15 10 56.1	1	48	50.4	
WARPJ0216.5–1747:R1	02 16 32.22	–17 45 17.2	3	115	7.2	
WARPJ0228.1–1005:R1	02 28 11.93	–10 05 32.7	4	5	7.0	BCG
WARPJ0348.1–1201:R1	03 48 09.29	–12 01 59.0	1	26	39.9	cluster member
WARPJ0951.7–0128:R1	09 51 46.39	–01 28 32.8	4	10	6.2	cluster member & star in error circle
WARPJ1407.6+3415:R1	14 07 45.46	+34 15 27.2	4	62	0.27	may be a sidelobe of another source
WARPJ1415.1+3612:R1	14 15 10.87	+36 12 07.0	6	5	5.4	
WARPJ1415.3+2308:R1	14 15 18.39	+23 08 39.6	4	18	8.7	
WARPJ1416.4+2315:R1	14 16 27.79	+23 15 35.3	10	12	4.1	BCG?
WARPJ1418.5+2511:R1	14 18 32.57	+25 12 03.9	1	65	38.9	
WARPJ1501.0–0824:R1	15 01 03.22	–08 24 39.9	6	23	9.6	
WARPJ2038.4–0125:R1	20 38 24.76	–01 24 02.1	21	100	7.9	Very extended
WARPJ2038.4–0125:R2	20 38 35.49	–01 25 58.4	1	100	31.1	
WARPJ2108.6–0507:R1	21 08 38.81	–05 07 43.4	9	22	3.7	
WARPJ2108.8–0516:R1	21 08 48.87	–05 16 05.1	3	41	9.6	
WARPJ2146.0+0423:R1	21 46 05.92	+04 22 44.1	11	30	3.6	
WARPJ2239.6–0543:R1	22 39 40.32	–05 43 23.0	6	14	8.4	BCG
WARPJ2302.8+0843:R1	23 02 48.10	+08 43 50.8	1	0	25.6	
WARPJ2320.7+1659:R1	23 20 44.42	+17 00 18.9	10	41	2.8	background AGN?

This figure "f2\_p1.png" is available in "png" format from:

<http://arxiv.org/ps/astro-ph/0112190v3>

This figure "f3\_p1.png" is available in "png" format from:

<http://arxiv.org/ps/astro-ph/0112190v3>



This figure "f2\_p2.png" is available in "png" format from:

<http://arxiv.org/ps/astro-ph/0112190v3>

This figure "f3\_p2.png" is available in "png" format from:

<http://arxiv.org/ps/astro-ph/0112190v3>

This figure "f2\_p3.png" is available in "png" format from:

<http://arxiv.org/ps/astro-ph/0112190v3>

This figure "f3\_p3.png" is available in "png" format from:

<http://arxiv.org/ps/astro-ph/0112190v3>

This figure "f2\_p4.png" is available in "png" format from:

<http://arxiv.org/ps/astro-ph/0112190v3>

This figure "f3\_p4.png" is available in "png" format from:

<http://arxiv.org/ps/astro-ph/0112190v3>

This figure "f2\_p5.png" is available in "png" format from:

<http://arxiv.org/ps/astro-ph/0112190v3>

This figure "f3\_p5.png" is available in "png" format from:

<http://arxiv.org/ps/astro-ph/0112190v3>



This figure "f2\_p6.png" is available in "png" format from:

<http://arxiv.org/ps/astro-ph/0112190v3>

This figure "f3\_p6.png" is available in "png" format from:

<http://arxiv.org/ps/astro-ph/0112190v3>

This figure "f2\_p7.png" is available in "png" format from:

<http://arxiv.org/ps/astro-ph/0112190v3>

This figure "f3\_p7.png" is available in "png" format from:

<http://arxiv.org/ps/astro-ph/0112190v3>

This figure "f2\_p8.png" is available in "png" format from:

<http://arxiv.org/ps/astro-ph/0112190v3>

This figure "f3\_p8.png" is available in "png" format from:

<http://arxiv.org/ps/astro-ph/0112190v3>

This figure "f2\_p9.png" is available in "png" format from:

<http://arxiv.org/ps/astro-ph/0112190v3>

This figure "f3\_p9.png" is available in "png" format from:

<http://arxiv.org/ps/astro-ph/0112190v3>



This figure "f2\_p10.png" is available in "png" format from:

<http://arxiv.org/ps/astro-ph/0112190v3>

This figure "f3\_p10.png" is available in "png" format from:

<http://arxiv.org/ps/astro-ph/0112190v3>

This figure "f2\_p11.png" is available in "png" format from:

<http://arxiv.org/ps/astro-ph/0112190v3>

This figure "f3\_p11.png" is available in "png" format from:

<http://arxiv.org/ps/astro-ph/0112190v3>

This figure "f3\_p12.png" is available in "png" format from:

<http://arxiv.org/ps/astro-ph/0112190v3>

This figure "f3\_p13.png" is available in "png" format from:

<http://arxiv.org/ps/astro-ph/0112190v3>

This figure "f3\_p14.png" is available in "png" format from:

<http://arxiv.org/ps/astro-ph/0112190v3>

This figure "f3\_p15.png" is available in "png" format from:

<http://arxiv.org/ps/astro-ph/0112190v3>



This figure "f3\_p16.png" is available in "png" format from:

<http://arxiv.org/ps/astro-ph/0112190v3>

This figure "f3\_p17.png" is available in "png" format from:

<http://arxiv.org/ps/astro-ph/0112190v3>

This figure "f3\_p18.png" is available in "png" format from:

<http://arxiv.org/ps/astro-ph/0112190v3>

This figure "f3\_p19.png" is available in "png" format from:

<http://arxiv.org/ps/astro-ph/0112190v3>

This figure "f3\_p20.png" is available in "png" format from:

<http://arxiv.org/ps/astro-ph/0112190v3>